AD-A120 769 FRACTURE ANALYSIS OF REACTION-BONDED SILICON NITRIDE TURBINE SHROUDS(U) ARMY MATERIALS AND MECHANICS RESEARCH CENTER WATERTOWN MA D R MESSIER ET AL. JUN 82 1/1

UNCLASSIFIED AMMRC-TR-82-43 F/G 1/3 NL

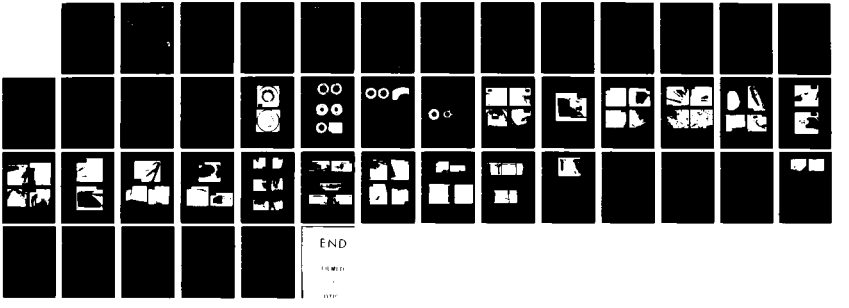

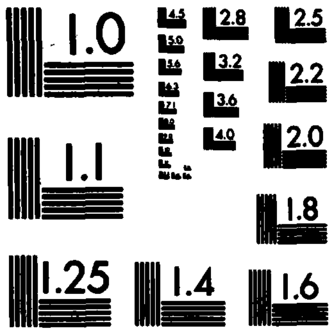

MICROCOPY RESOLUTION TEST CHART
NATIONAL BUREAU OF STANDARDS-1963-A

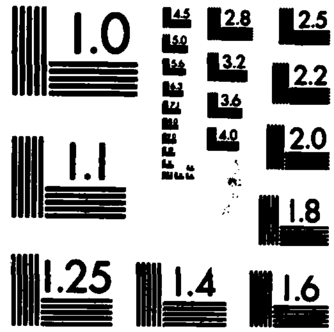

MICROCOPY RESOLUTION TEST CHART
NATIONAL BUREAU OF STANDARDS-1963-A

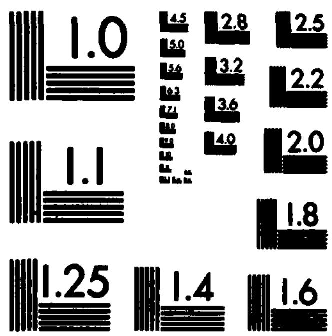

MICROCOPY RESOLUTION TEST CHART
NATIONAL BUREAU OF STANDARDS-1963-A

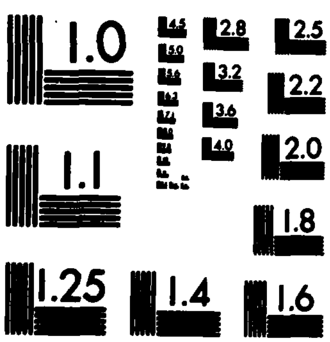

MICROCOPY RESOLUTION TEST CHART
NATIONAL BUREAU OF STANDARDS-1963-A

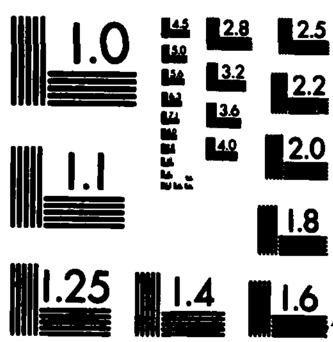

MICROCOPY RESOLUTION TEST CHART
NATIONAL BUREAU OF STANDARDC-1963-A

AMMRC TR 82-43

AD

FRACTURE ANALYSIS OF REACTION-BONDED SILICON NITRIDE TURBINE SHROUDS

DONALD R. MESSIER, LISELOTTE J. SCHIOLER, GEORGE D. QUINN, and JAMES C. NAPIER

CERAMICS RESEARCH DIVISION

JUNE 1982

ARMY MATERIALS AND MECHANICS RESEARCH CENTER
Watertown, Massachusetts 02172

The findings in this report are not to be construed as an official Department of the Army position, unless so designated by other authorized documents.

Mention of any trade names or manufacturers in this report shall not be construed as advertising nor as an official indorsement or approval of such products or companies by the United States Government.

DISPOSITION INSTRUCTIONS

Destroy this report when it is no longer needed.
Do not return it to the originator.

UNCLASSIFIED

SECURITY CLASSIFICATION OF THIS PAGE (When Data Entered)

REPORT DOCUMENTATION PAGE		READ INSTRUCTIONS BEFORE COMPLETING FORM
1. REPORT NUMBER AMMRC TR 82-43	2. GOVT ACCESSION NO. AD-A120 269	3. RECIPIENT'S CATALOG NUMBER
4. TITLE (and Subtitle) FRACTURE ANALYSIS OF REACTION-BONDED SILICON NITRIDE TURBINE SHROUDS		5. TYPE OF REPORT & PERIOD COVERED Final Report 6. PERFORMING ORG. REPORT NUMBER
7. AUTHOR(s) Donald R. Messier, Liselotte J. Schioler, George D. Quinn, and James C. Napier*		8. CONTRACT OR GRANT NUMBER(s)
9. PERFORMING ORGANIZATION NAME AND ADDRESS Army Materials and Mechanics Research Center Watertown, Massachusetts 02172 DRXMR-MM		10. PROGRAM ELEMENT, PROJECT, TASK AREA & WORK UNIT NUMBERS D/A Project: 1L763702 DG1105 AMCMS Code: 623702.G1100
11. CONTROLLING OFFICE NAME AND ADDRESS U. S. Army Materiel Development and Readiness Command, Alexandria, Virginia 22333		12. REPORT DATE June 1982 13. NUMBER OF PAGES 38
14. MONITORING AGENCY NAME & ADDRESS(if different from Controlling Office)		15. SECURITY CLASS. (of this report) Unclassified 15a. DECLASSIFICATION/DOWNGRADING SCHEDULE

16. DISTRIBUTION STATEMENT (of this Report)

Approved for public release; distribution unlimited.

17. DISTRIBUTION STATEMENT (of the abstract entered in Block 20, if different from Report)

18. SUPPLEMENTARY NOTES

*Solar Turbine International, San Diego, California

19. KEY WORDS (Continue on reverse side if necessary and identify by block number)

Silicon nitride	Mechanical properties
Ceramics	Fracture mechanics
Gas turbine engine	Failure analysis

20. ABSTRACT (Continue on reverse side if necessary and identify by block number)

(SEE REVERSE SIDE)

DD FORM 1 JAN 73 1473 EDITION OF 1 NOV 65 IS OBSOLETE

UNCLASSIFIED

SECURITY CLASSIFICATION OF THIS PAGE (When Data Entered)

Block No. 20

ABSTRACT

Reaction-bonded silicon nitride turbine shrouds were examined after engine rig testing to determine failure mechanisms and evaluate material quality. Bend test specimens machined from the shrouds were approximately equal in strength to specimens cut from flat billets of virgin material. While most component and bend specimen fractures initiated at surfaces, internal origins were observed in some cases. Fracture mechanics analysis of the bend test data yielded a value of K_{Ic} = 1.79 MN/m$^{3/2}$ in agreement with literature data. Fracture mirror measurements indicated that shrouds failed at stresses approximately three times less than bend specimens. Probable causes for this were gross machining defects, size effects, and possible residual stresses.

m cubed/2

CONTENTS

I. INTRODUCTION

The work reported here is part of a program, "MM&T, High Temperature Turbine Nozzle for 10-kW Power Unit," sponsored by the Mobility Equipment Research and Development Command (MERADCOM), Fort Belvoir, Virginia, with the engine testing and development being conducted by Solar Turbines International, San Diego, California. The objective of the program is to develop manufacturing methods for ceramic nozzle vanes. AMMRC is providing consulting advice and characterization of ceramic candidate materials.

Failure analysis is an important part of any such program. When material failures occur, it is essential to determine what caused them, i.e., improper design, uncontrolled testing conditions, or materials not meeting specifications as to quality, surface finish, or dimensional tolerances. The data base thus generated is required to set specifications and quality control standards, and also for the design of similar components in future systems.

The reaction-bonded silicon nitride (RBSN) shrouds examined in this study were furnished to AMMRC by Solar after engine rig testing at their facility. Details of the engine testing are given in a report recently published by Solar.[1] The failure analysis work was conducted at AMMRC.

II. EXPERIMENTAL PROCEDURES

A. Engine Rig Testing

As indicated in the Introduction, details of testing of the shrouds appear in another report.[1] Consequently, only a brief summary of the results is presented here.

The shrouds that were tested were obtained from a commercial vendor.* They were fabricated by machining silicon powder compacts to the desired shape, and nitriding the resulting components to convert them to RBSN. Finish machining was minimal. Characterization data on the material appears in section III.

Most of the shrouds were tested in an engine simulator test rig. The component identification numbers that we have used are the ones given by Solar.[1] An example of a typical designation follows:

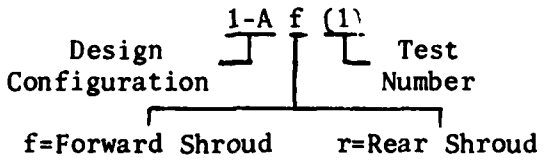

The shrouds labeled 1-A, 1-B, 1-D, and 2-C were tested in the engine simulator test rig. Testing consisted of up to 4 hours steady-state operation at a turbine inlet temperature (TIT) of 927°C (1700°F) followed by up to 500 thermal shock cycles for shrouds that survived the steady-state test. The thermal shock cycle for the rear shroud involved heating from 677°C (1250°F) to 1066°C (1950°F) in 30 seconds followed by cooling to the starting temperature in 30 seconds. The cycle was the same for the forward shroud except that the minimum temperature was 538°C (1000°F) and the maximum was 882°C (1620°F).

*NC-350 Reaction-Bonded Silicon Nitride, Norton Co., Worcester, Massachusetts

1. NAPIER, J. C., METCALFE, A. G., and DUFFY, T. E. *Application of Ceramic Nozzles to 10-kW Engine.* Solar Turbine International, Report S.O. 6-4375-7, 1979. (AD-A081-184)

The shroud designated 4-Er (7) was tested in the engine test rig in the configuration illustrated in Figure 1. Figure 1a is a rear view of the assembly with the rear shroud in place, and Figure 1b is the same view with the rear shroud removed. In this test, the forward shroud was siliconized silicon carbide and the vanes were hot-pressed silicon nitride. The testing included 19 stop/start cycles and the maximum TIT at full load was 904°C (1660°F). A summary of the testing follows:

Operating Condition	Time at Load (hr)
Calibration	5
50% Load	24
0% Load	4
100% Load	10.5
75% Load	6.5
Total	50

B. Fabrication of Bend Test Specimens

Bend test specimens were machined from the engine-tested shrouds. The bend bars were rectangular parallelepipeds measuring 2.2 x 2.8 x 50.9 mm. These dimensions were chosen to give specimens sufficiently large for testing while at the same time maximizing the number obtainable from each component. The orientations of the bend specimens with respect to the shroud were similarly selected to maximize the number obtainable from each shroud. Machining of the bend bar surfaces and chamfering of their edges were done according to the procedure described by Quinn.[2] That procedure involved machining with either a 220- or 280-grit diamond wheel such that the striations were parallel to the long axis of the bend specimen. The final finish removal rate was 1.5×10^{-3} mm per pass. The four long edges were chamfered at 45° to a depth of 0.15 mm.

The bend specimens were tested at room temperature in four-point loading with inner and outer spans of 15.2 and 30.4 mm. The crosshead speed used was 0.05 mm/min. The bend specimens were long enough so that on occasion two breaks per specimen were possible. In such cases, care was taken to insure that the previously stressed portion of the sample was not reinserted into the inner gauge length.

C. Fracture Analysis

Fracture surfaces of all shrouds and bend bars were examined carefully both visually and by optical microscopy. Many of the fracture surfaces were further examined by scanning electron microscopy with emphasis on the identification of fracture origins and critical defects.

For cases in which mirrors were clearly defined, fracture mirror radii were measured with a reticular lens on a binocular microscope. Flaw sizes were determined from measurements on scanning electron photomicrographs of fracture surfaces of bend specimens.

2. QUINN, G. D. *Characterization of Ceramic Turbines After Long-Term Environmental Exposure.* Army Materials and Mechanics Research Center, AMMRC TR 80-15, April 1980.

III. RESULTS

A. Shroud Testing

The engine simulator test rig results are summarized in Table 1.[1] As seen in that table, all failures, except one (1-D), were associated with rig problems of the sort to be expected in such preliminary testing. Analysis of such failures is nevertheless instructive in establishing sources and mechanisms of failure.

Figures 2 through 6 are photographs of the RBSN shrouds as they appeared after testing in the engine simulator rig. One shroud (1-Ar, Figure 2) survived intact with the remainder showing behavior ranging from subcritical cracking to catastrophic failure.

Figures 7 through 10 are drawings of the failed shrouds detailing the cracking patterns that were observed in them. All of these figures are rear views of forward shrouds with the vane indents omitted for clarity. As indicated, each piece of a shroud was numbered and locations where cracks started or ended were designated with letters. This system was followed consistently in labeling subsequent detailed pictures. For example, the designation "1-Af (1) a1" refers to location "a" on piece No. 1 of shroud 1-Af (1).

Fracture origins (labeled "o") and crack propagation directions (indicated by arrows) were identified insofar as possible by examination of fracture surfaces visually and by low-power optical microscopy.[3-7] The arrows were omitted when the crack propagation direction was uncertain. Fracture initiated at the surface on the inside forward corner of each

Table 1. RESULTS OF TESTING OF CERAMIC NOZZLES IN ENGINE SIMULATOR TEST RIG (Ref. 1)

Nozzle	Test Sequence	Results
1-A	2 hours steady state at 927°C (1700°F) TIT.	Forward shroud fractured. Inadvertent sea salt ingestion caused corrosion on seal plate and interference that led to failure.
1-B	4 hours steady state at 927°C (1700°F) TIT and 167 thermal shock cycles.	Forward shroud fractured in thermal shock test. Overheating of diffuser housing caused misfit that overstressed shroud.
2-C	4 hours steady state at 927°C (1700°F) TIT followed by flameout with cold air supply on.	Forward shroud fractured. Cause appeared to be thermal binding at joint between combustor can and outer shroud retaining ring and/or thermal stress.
1-D	4 hours steady state at 927°C (1700°F) TIT and 500 thermal shock cycles.	Subcritical crack in forward shroud apparently caused by thermal stress.

3. FRECHETTE, V. D. *The Fractology of Glass* in Introduction to Glass Science. L. D. Pye, H. J. Stevens, and W. C. LaCourse, ed., Plenum Press, New York, 1978, p. 227-231.
4. FRECHETTE, V. D. *Fractography and Quality Assurance of Glass and Ceramics* in Quality Assurance in the Ceramic Industry. V. D. Frechette, L. D. Pye, and J. S. Reed, ed., Plenum Press, New York, 1978, p. 227-236.
5. RICE, R. W. *Fracture Topography of Ceramics* in Surfaces and Interfaces of Glass and Ceramics. V. D. Frechette, W. C. LaCourse, and V. L. Burdick, ed., Plenum Press, New York, 1974, p. 439-472.
6. RICE, R. W., MECHOLSKY, J. J., FREIMAN, S. W., and MOREY, S. M. *Failure Causing Defects in Ceramics: What NDE Should Find.* Naval Research Laboratory, NRL Memorandum Report 4075, 1979.
7. MECHOLSKY, J. J., FREIMAN, S. W., and RICE, R. W. *Fracture Surface Analysis of Ceramics.* J. Mater. Sci., v. 11, 1976, p. 1310-1319.

shroud with the exception of one case, shroud 1-Bf (2) (Figure 8), where an origin was found at a bolt hole.

Shroud 4-Er (7), which failed during engine rig testing, is shown in Figures 11 and 12. During testing of that shroud, combustion problems occurred which were attributed to compressor surge.[1] When the rig was disassembled for examination after 33 hours, the crack "g-h" (Figure 12) was discovered. Piece No. 5 remained in place, however, and testing was continued. After 50 hours, the exhaust scroll was found to be partially collapsed, the additional cracking in the rear shroud (Figure 12) was observed, and the test was terminated. The cause of failure at that point was believed to be excessive stress generated by buckling of the exhaust scroll.

Figures 13 through 29 are optical macrographs and scanning electron photomicrographs of shroud fracture surfaces illustrating various features that were observed.

The fracture surfaces shown in Figure 13a and b exhibit the classical features found on such surfaces,[3,4] i.e., a smooth "mirror" region near the origin (point "a" in Figure 13b), a coarser "mist" region beyond the mirror, and the coarse "hackle" region beyond the mist. These features are particularly well-defined in Figure 16a, and the corresponding regions labeled for reference. Note that the "river" patterns in the hackle region may be traced back to the fracture origin which, as already mentioned, is at an inside corner of the shroud. Figure 14 shows another part of shroud 1-Af (1); the hackle lines at the left indicate that the crack emerged (rather than initiated) at that location.

Figures 15 through 19 show various features of the fracture of shroud 1-Bf (2). Figure 15 illustrates one problem in post-mortem fracture analysis; the chip in the lower corner in (a) is not duplicated in (b) suggesting that it occurred in handling after the fracture event. The markings in Figures 15 through 19 again indicate that fracture initiated at inside corners. The large hackle marks in Figure 16 suggest catastrophic failure and Figure 17 shows a large pore near the fracture origin. Also present in the same region are large surface gouges that are probably left over from machining of the component. Figures 18 and 19 show surfaces near the origin of the only fracture that started at a hole. Prominent in Figure 18 are Wallner lines, the semicircular markings some distance away from location "i". These features are always concave toward the fracture origin.[3,4] Figure 19 shows a possible chip or machining defect (near "i") at which fracture could have originated.

Figures 20 through 24 show fracture surfaces on shroud 2-Cf (4). The chip near the lower left corner in Figure 20b probably occurred during handling, and fracture again initiated at the inside corner. Evident in Figure 21 is a large gouge on the edge of the component near the fracture origin as well as a large inclusion in the same region. Fracture surfaces near origin "c" are shown in Figure 22 and 23. The groove on the corner near "c" (Figure 23) may have caused failure. The region near "d" in which a subcritical crack originated is shown in Figure 24. Note the especially small fracture mirror associated with this origin. Figure 25 shows clearly the type of large machining striations that were found in several instances.

The results of fractographic examination of shroud 4-Er (7) are shown in Figures 26 through 29. This was the only shroud in which internal fracture origins were observed. Figure 26 shows the origin for the fracture that occurred near point "g", shown in Figure 12, after 33 hours. The Wallner lines and hackle markings clearly indicate an internal origin. The fracture origin near "b" is shown in Figures 26 and 27. Interpretation of this fracture was more difficult than in previous cases. Examination of the fracture surfaces, however, suggests that the porous area near "y" (Figure 28a and c) was the fracture-initiating defect. The crack seen in Figure 28b and d appears to have initiated near "y"

supporting the above suggestion. Figure 29 shows the region near a third possible origin in shroud 4-Er (7). Fracture may have initiated near the chip in Figure 29b, but the hackle lines in Figure 29a indicated that the origin may have been to the right of the point indicated by the arrow.

B. Mechanical Testing

Table 2 summarizes the data from bend test specimens machined from the six shrouds that had been engine tested. The density data given in Table 2 were computed from measurements of the masses and dimensions of the bend bars. Density data were not obtained for shroud 4-Er (7). Density varied little from one shroud to another, and the low standard deviations for the individual shroud data indicate that the material was uniform throughout.

All the specimens, with the exception of five from shroud 4-Er (7), were tested with as-machined surfaces. As noted in Table 2, fracture origins were, when possible, identified as either machining or "native" (material) defects. In the remaining cases, failure resulted

Table 2.. COLLECTED FRACTURE DATA FROM MECHANICAL TESTING OF SPECIMENS MACHINED FROM RBSN SHROUDS

Shroud	Stress (MPa)	Source	Location	Shroud	Stress (MPa)	Source	Location	Shroud	Stress (MPa)	Source	Location
1-Af(1)	208	M/N	C	1-Df(5)	126	N	S	4-Er(7)	199	M	S
ρ=2,490±10	211	N	S	ρ=2,490 ±10	185	M/N	C	(Machined	202	U	S
kg/m^3	218	N	S	kg/m^3	196	M	I	Surfaces)	222	U	U
	229	N	C		200	M	U		222	M/N	C
	247	N	S		203	M	S		238	M	C
	260	N	S		210	N	I/C		244	U	C
	270	M/N	S		216	M	C		249	N	C
	270	M/N	S		217	M	C		274	U	U
	274	U	U		224	U	U		280	U	C
	295	N	S		232	N	S		289	M	C
	295	N	S		234	M/N	S		297	M	C
	311	U	S		237	M/N	C		299	U	C
	343	U	U		244	N	S		299	M	S
	399	U	U		246	N	S		302	U	C
					247	N	S		306	U	C
1-Bf(2)	172	M	C		251	U	S		314	N	I
ρ=2,470 ±10	181	M/N	S		251	N	S		317	U	S
kg/m^3	204	M	S		255	M/N	S		326	U	S
	251	N	C		284	M	C		328	M	C
	257	M	C		291	N	S		344	M	C
	263	M	C		299	M/N	S		376	U	S/I
	268	M	C		305	U	C		377	M	C
	320	U	S		307	N	S				
	372	U	S		309	M	C	4-Er(7)	73	N	S
								(As-Received	83	N	U
2-Cf(4)	•	-	S	1-Ar(1)	163	M	C	Surfaces)	95	N	S
ρ=2,470±10	•	-	-	ρ=2,520±10	233	M/N	C		101	N	C/S
kg/m^3	232	N	S	kg/m^3	237	N	S		124	N	S
	271	U	S		238	M	C				
	273	N	I		262	M	C				
	286	N	I		266	U	C				
	293	N	I		269	M	C				
	298	M	C		282	N	C				
	299	M	S		283	U	C				
	321	U	C		299	N	S				
	345	U	S		305	M	C				
					306	N	I				
					307	N	I				
					363	N	S				
					364	U	U				
					400	M	I				

*Specimen failed from large crack at undetermined low stress.
Key to symbols: C, Corner; I, Interior; M Machining Defect; N, Material Defect; S, Surface; U, Unkno-

either from a combination of the two or from an unidentifiable source. Note also in Table 2 that the bend bar fractures generally originated at surfaces and internal origins were found in only a few instances.

Figures 30 through 33 show examples of each type of identifiable flaw observed at fracture origins in bend specimens. Native material defects were generally porous areas as shown in Figure 30. Gouges from machining similar to the ones shown in Figure 31 and 32 were associated with failures attributed to machining defects. The machining defect shown in Figure 32 was associated with porosity, and it was thus categorized as "mixed". An example of one of the few defects (a subsurface pore) causing failure to originate internally is given in Figure 33.

IV. DISCUSSION OF RESULTS

A. Shroud Testing

The three shrouds (1-A, 1-B, and 2-C) that failed completely during testing in the engine simulator rig showed similar behavior. Failure occurred typically in tension at the inner surface with the origins being more or less diametrically opposite each other. Such behavior would be expected of a hoop-shaped specimen; as soon as one crack opened, the tensile stress would be highest diametrically opposite to it.

In the example shown in Figure 9, the second crack may have originated at a large defect, rather than at the maximum stress location, or failure could have originated simultaneously at locations "a" and "c". The latter seems more plausible since the subcritical crack at "d" is diametrically opposite a point midway between "a" and "c". It is impossible to deduce unequivocally from the fracture patterns in Figures 7 through 9 which fracture occurred first. For the case in which failure was catastrophic, however, it appears that the first crack initiated at "a" (Figure 8). That crack has more branches than the one starting at "e", suggesting that the stress was higher at "a",[5] and the branch traveling circumferentially counterclockwise traveled much further than the intersecting crack from location "e". The crack starting at "e" may also have traveled slightly farther before branching, again indicating that the failure stress may have been lower at that point.[6] It may also be noted that the catastrophic cracking in shroud 1-Bf (2) (Figure 8) indicates that it failed at a higher stress level than the other two (Figures 7 and 9).

The fracture behavior of shroud 4-Er (7) which endured 50 hours of engine rig testing was markedly different than that described above. Crack initiation sites (if any) and propagation directions in the vicinity of locations "c" and "d" in Figure 12 were impossible to establish with certainty. The two identifiable fracture origins both appeared to be internal ones. It is likely that those failures resulted from thermal stress during heating; such a situation would induce compressive stresses on the outside, and corresponding corresponding tensile stresses on the inside of the part.

B. Mechanical Testing

Although the shrouds were tested in an oxidizing environment for up to 50 hours at temperatures (900°C) at which internal oxidation may have degraded properties[8] none of the failures appear to have been corrosion-related. In support of this conclusion are the data summarized in Figure 34 which shows the mean strength values for each set of bend specimens (except for the five tested with as-received surfaces) as well as baseline data

8. *Ceramic Gas Turbine Engine Demonstration Program.* AiResearch Manufacturing Co., Report 76-212188(14), 1979.

obtained by Quinn[2] for specimens machined from flat billets of virgin material. Our specimens were prepared and tested in the same manner as Quinn's. His material, however, was furnished by the manufacturer in the form of simple disks (not component shapes) 190-mm diameter x 4.5-mm thick. The number (n) given in Figure 34 for each shroud is the total number of breaks obtained on specimens from that particular component. Also shown are value. of the Weibull modulus (m),[9] and standard deviation for each set of results.

The significance of the difference between the mean strength for each shroud and the baseline value was evaluated by means of a two-tailed t test.[10] In only one case (shroud 1-Df (5)) was the difference significant (highly significant at the 99.9% level); other differences were statistically insignificant (<95% to <50%). These results are encouraging, for they indicate that material can be produced in a complex shape with strength equal to that of a simpler form.

Figures 35 and 36 show the bend test data plotted according to a normal distribution.[10] It is evident that they fit such a distribution well, justifying the use of statistical comparative tests that assume such a distribution. It is also noteworthy that there is no apparent "cutoff" at the lower stress levels, as might be expected if there were a minimum "proof" strength.

Figure 37 shows the data plotted according to the Weibull distribution which one would expect to obtain from theoretical considerations.[9] Again the fit is satisfactory. Also given in Figure 37 are Weibull modulus values obtained by both least squares (LS)[10] and maximum likelihood estimator (MLE)[11] techniques. The advantage of the MLE technique is that it gives error bounds while the LS technique does not.

Table 3 summarizes the calculated results of statistical parameters for the data plotted in Figures 35 through 37. Note that the modulus value of 5.6 obtained by the LS technique is well within the MLE bounds of m = 4.4 to 6.0 at the 90% confidence level.

Table 3. STATISTICAL PARAMETERS OF FRACTURE ANALYSIS

Distribution	Parameter	Value
Normal	RMS Error	0.020
	Mean Stress (MPa)	270
	90% Confidence Limits	261-279
	Standard Deviation (MPa)	54
	90% Confidence Limits	48-61
Weibull (MLE Technique)	RMS Error	0.028
	Weibull Slope (m)	5.41
	90% Confidence Limits	4.68-6.11
	Characteristic Value (MPa)	292
	90% Confidence Limits	282-302

9. WEIBULL, W. A. *Statistical Distribution Function of Wide Applicability.* J. Appl. Mech., v. 18, no. 3, 1951, p. 293-297.
10. STEELE, R. G. D., and TORRIE, J. H. *Principles and Procedures of Statistics.* McGraw-Hill, New York, 1960.
11. MASON, D., NEAL, D., and LENOE, E. *Statistical Data Evaluation Procedures.* Army Materials and Mechanics Research Center, Technical Report (to be published).

Of some interest in further defining fracture mechanisms is whether or not significant differences existed among bend specimen fractures originating from the different defect types identified by microscopic analysis. For this purpose, the data in Table 2 was separated into groups corresponding respectively to failures from material and machining defects. Shown in Table 2 are numerous cases in which the source of failure could not be identified unequivocally. In view of this difficulty, the data were categorized in two different ways for statistical testing of the hypothesis that machining damage reduced material strength.

Although it is recognized that the procedure used to categorize defects may be biased, such categorization is still felt to be useful.

Table 4 summarizes the results of that statistical analysis. The column labeled "All Specimens" contains all of the data categorized according to failures associated with machining damage (coded M or M/N in Table 2) or failures ascribed to material defects or unknown causes. The column labeled "Selected Data" includes data only on failures unequivocally caused by machining or material defects (coded M and N in Table 2). While comparison of the results categorized in the first way indicates that machining damage reduces strength at a highly significant level, the second comparison indicates no significant difference. While the mean strengths associated with machining damage are lower than those associated with material defects for the first of the data treatments, it must be concluded that the machining done in preparation of the bend test specimens had minimal effect on strength.

Table 4. EFFECT OF MACHINING DAMAGE ON STRENGTH OF RBSN BEND TEST SPECIMENS AS DETERMINED FROM A SINGLE-TAILED t TEST

Parameter	All Specimens		Selected Data	
Failure Origin	Machining	Material	Machining	Material
No. of Tests	39	55	29	29
Mean Fracture Stress (MPa)	256	279	263	262
Standard Deviation (MPa)	±55	±54	±59	±45
t	2.109		0.075	
Level of Significance	>97.5<99%		Insignificant	

C. Fracture Mechanics

Fracture surfaces of most fine-grained materials exhibit certain characteristic features: mirror, mist, and hackle.[3,4] The fracture stress, σ_f, is empirically related to the mirror radius by:

$$\sigma_f = A/r^{1/2} \qquad (1)$$

where A is a constant.[7,12] Mirror radii were measured for 35 of the 72 fracture specimens (some of the mirrors were too ill-defined to measure) by use of a reticular lens on a binocular microscope. The value taken for the radius was the average of measurements in several directions of the distance from the fracture source to the mirror-mist boundary.

12. KIRCHNER, H. P., and KIRCHNER, J. W. *Fracture Mechanics of Fracture Mirrors.* J. Am. Ceram. Soc., v. 62, no. 3-4, 1979, p. 198-202.

Figure 38 is a plot of fracture stress versus mirror radius. A least squares analysis of the data yielded a value of A = 3.92 $MN/m^{3/2}$. This value is in reasonable agreement with the value of 4.2 $MN/m^{3/2}$ reported by Kirchner et al.[13] for a different grade of RBSN, and also with that of 3.19 $MN/m^{3/2}$ reported by Larsen and Walther[14] for the same type of material (NC-350) investigated in this study.

An important material parameter, the critical stress intensity factor, can be obtained by means of fractographic analysis. This factor can be expressed as follows:

$$K_{Ic} = Y\sigma_f c^{1/2} \qquad (2)$$

where Y is a geometric constant related to the flaw shape and loading mode, and c is the flaw size.

For the case of a shallow, semicircular surface crack in a beam in bending, Y will vary along the crack front periphery, ranging in value from 1.35 at the surface to 1.16 at the deepest interior point.[15] The selection of a value of Y to use in estimating K_{Ic} must consider the fact that our values for flaw sizes (c) are averages of measurements in several directions. Acknowledging this, we selected an average value of Y = 1.26 as did Mecholsky et al.[7]*

A detailed characterization of the flaws was done for 18 fracture specimens (all from shroud 4-Er (7)) and a value of K_{Ic} = 1.76 ± 0.25 $MN/m^{3/2}$ was obtained from a least-squares analysis of a plot of stress versus flaw size (Figure 39). This value compares favorably to others obtained on the same material by various techniques, i.e., 2.06 $MN/m^{3/2}$ by double torsion,[14,16] and 1.73 - 2.07 $MN/m^{3/2}$ [16] and 1.87 $MN/m^{3/2}$[17] by means of controlled flaw experiments.

D. Shroud Failure

Of considerable interest is the estimation of stress levels which caused failure of the shrouds. Such estimates can be made using Equation (1) from mirror measurements on fracture surfaces, given that the constant, A, has already been determined from the bend bar data. Although the bend tests were conducted at room temperature and the components failed at elevated temperatures (1100°C or less), it seems unlikely that the value of A would vary much over that temperature range. It is known that K_{Ic}, for the material that was tested, is essentially constant in this temperature regime,[17,18] and it has also been shown that K_{Ic} is proportional to A.[7]

*For the sake of clarity, it should be noted that Mecholsky et al.[7] defined their geometric constant somewhat differently than we have.

13. KIRCHNER, H. P., GRUVER, R. W., and SOTTER, W. A. *Fracture Stress - Mirror Size Relations for Polycrystalline Ceramics.* Phil. Mag., v. 33, no. 5, 1976, p. 775-780.
14. LARSEN, D. C., and WALTHER, G. C. *Property Screening and Evaluation of Ceramic Turbine Engine Materials.* IIT Research Institute, IITRI-D6614-ITR-30, Interim Technical Report 5, 1978.
15. SMITH, F. W., EMERY, A. F., and KOBAYASHI, A. S. *Stress Intensity Factors for Semicircular Cracks.* Trans. ASME, Series E, v. 89, 1967, p. 953-959.
16. LARSEN, D. C., and WALTHER, G. C. *Property Screening and Evaluation of Ceramic Turbine Engine Materials.* IIT Research Institute, IITRI-D6114-ITR, Interim Technical Report 6, 1978.
17. WILLS, R. R., MENDIRATTA, M. G., and PETROVIC, J. J. *Controlled Surface Flaw Initiated Fracture in Reaction-Bonded Si_3N_4.* J. Mater. Sci., v. 11, 1976, p. 1330-1334.
18. LARSEN, D. C. *Property Screening and Evaluation of Ceramic Turbine Engine Materials.* IIT Research Institute, IITRI-D6114-ITR-42, Interim Technical Report 7, 1979.

Table 5 summarizes the results of fracture mirror measurements (in cases where such measurements could be made) on failed shrouds, and fracture stresses calculated therefrom. All of these fractures initiated at surfaces, and it is apparent that the shrouds failed at much lower stresses than did the bend test specimens. This is consistent with probabilistic theories of strength[9] which indicate that failure stress is inversely proportional to surface area and/or volume. Supporting evidence for such an effect was given by Jones and Rowcliffe[19] who found that large rings (60 mm OD) of RBSN failed at significantly lower stresses than did small rings (30 mm OD). In our case, however, quantitative evaluation of any such size effect is impossible; information on the load and stress distribution during engine testing is unavailable.

The calculated fracture stress values in Table 5 agree well with the results in Table 2 for bend specimens tested with as-received surfaces. In the case of the shrouds, Figures 13, 15, 17, 21, and 23 show evidence of gross machining defects near fracture origins. Similar defects were suspected, but not observed clearly at fracture origins in bend bars with as-received surfaces. On the other hand, it has already been noted that numerous failures in bend specimens with machined surfaces were related to machining flaws (less severe that the above-mentioned ones), but statistical testing results were inconclusive as to whether or not such relatively minor flaws significantly lowered strength. Jones and Rowcliffe[19] similarly noted that their RBSN specimens frequently had machining grooves at fracture origins. In view of the foregoing discussion it appears that, at some level, the fracture strength of RBSN will be significantly degraded by the presence of surface machining flaws.

For shroud 4-Er (7), where internal fracture origins were found, estimates of failure stresses were impossible. As already indicated, it appears that these failures were caused by thermal stresses during heating, however, insufficient data exists to estimate quantitatively the magnitude of those stresses.

An additional complicating factor that should be considered is the likelihood of significant residual stresses in the components. For example, it was observed that during the initial cutting of a shroud to machine bend specimens, spontaneous cracks propagated throughout the piece. This occurred despite care taken to avoid impact or other abuse in the cutting process. Further evidence of residual stresses was that the shroud halves tended to "spring together" when the first cut was made through the cross section of one

Table 5. ESTIMATION BY EQUATION 1 OF STRESSES CAUSING COMPONENT FRACTURE

Component	Location	Mirror Radius (mm)	Calculated Fracture Stress (MPa)
1-Af (1)*	a	2.36	80
	b	1.64	96
1-Bf (2)*	a	1.05	120
	c	1.03	121
2-Cf (4)	a	1.57	98

*Two fracture origins on same component.

19. JONES, R. L., and ROWCLIFFE, D. W. *Tensile-Strength Distributions for Silicon Nitride and Silicon Carbide Ceramics.* Am. Ceram. Soc. Bull. v. 58, no. 9, 1979, p. 836-839.

of the ring-shaped pieces. The net effect of such residual stresses would be to lower the load-carrying capacity of the shrouds relative to the bend specimens. It is unlikely that the latter contained residual stresses because such stresses would have caused specimens to fail during machining.

V. SUMMARY

In summary, it may be concluded that:

1. Reaction-bonded silicon nitride (RBSN) may be fabricated into complex shapes, i.e., turbine shrouds, having mechanical properties equivalent to those of material produced in simpler forms.

2. Machining damage minimally reduced the strength of RBSN bend test specimens with high-quality surfaces.

3. RBSN shrouds failed at substantially lower stresses than bend test specimens. Probable causes for this include:

   a. gross machining defects in the shrouds,

   b. a size effect which would cause a larger piece (the shroud) to fail at a lower stress than a smaller one (bend specimen), and

   c. residual stresses in the shrouds.

VI. ACKNOWLEDGMENT

The authors are grateful to the Mobility Equipment Research and Development Command, Fort Belvoir, Virginia, for support of this work. Of particular assistance from that installation were J. P. Arnold and W. F. McGovern.

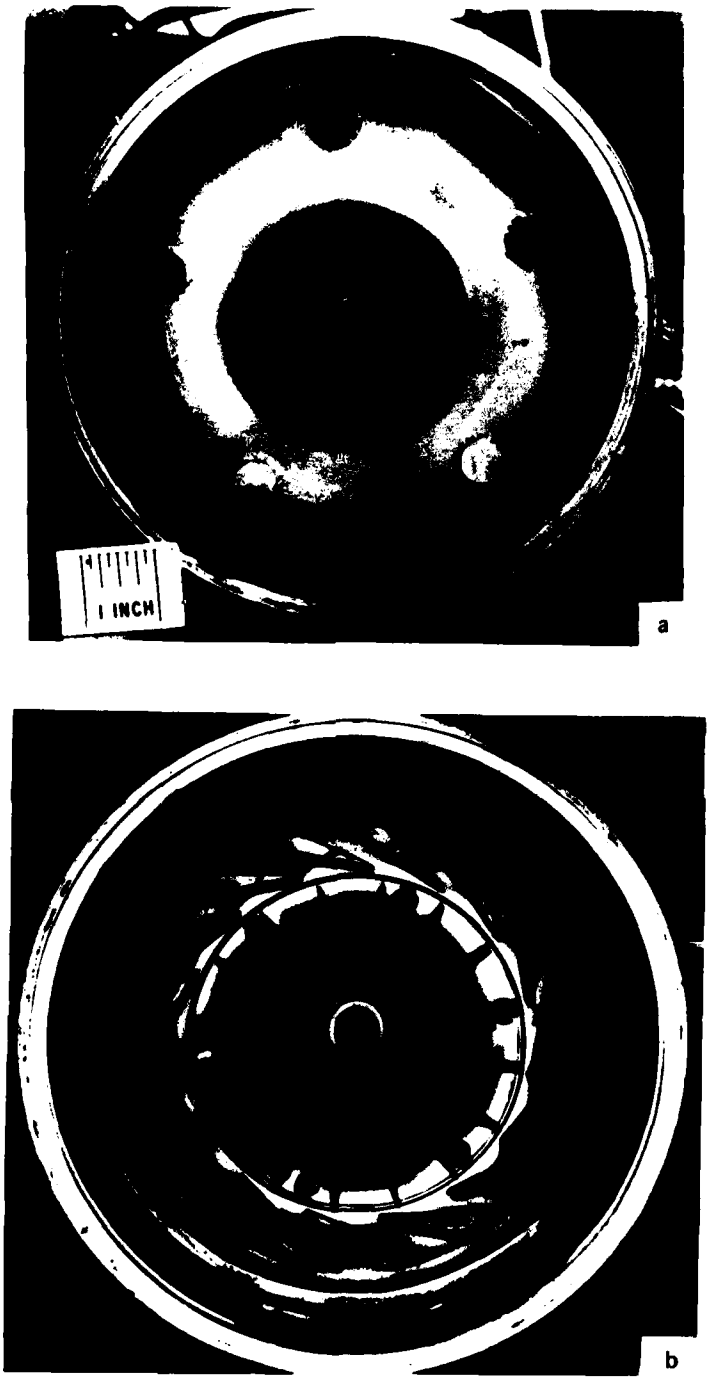

Figure 1. Rear view of engine test rig with (a) ceramic shroud in place and (b) with rear shroud removed.

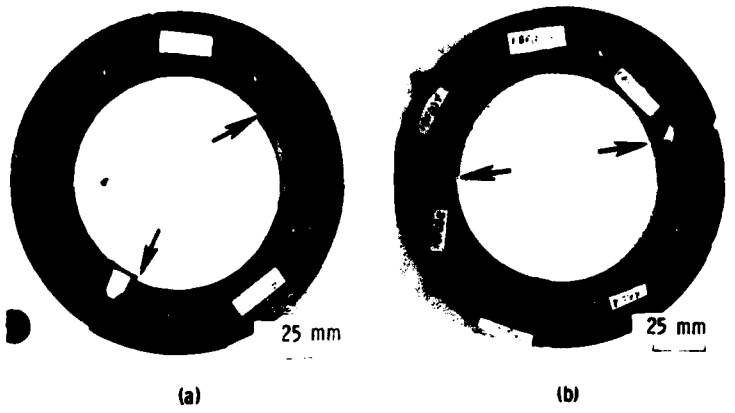

Figure 2. RBSN forward shrouds after testing in the 10-kW turbo alternator. (a) and (b) were tested in different runs. The arrows point to sites where fracture initiated.

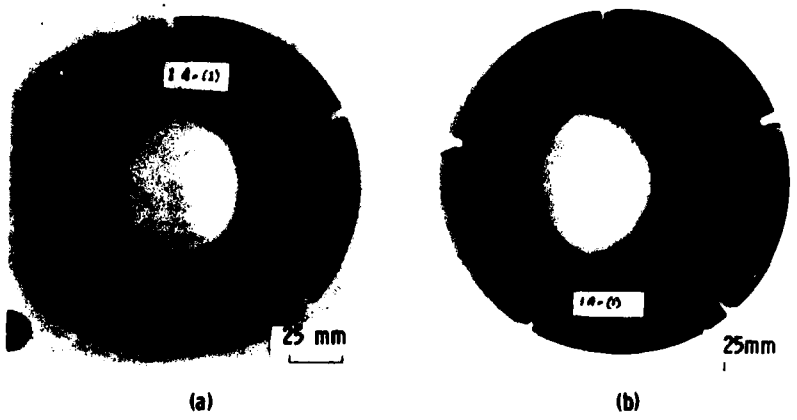

Figure 3. RBSN rear shroud after testing in the 10-kW turbo alternator with (a) front view and (b) rear view. This part was uncracked.

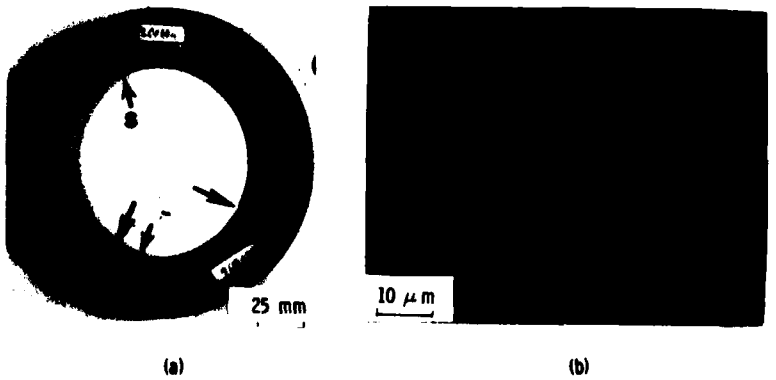

Figure 4. RBSN front shroud after testing in the 10-kW turbo alternator with (a) complete shroud and (b) detail near subcritical crack. The arrows point to sites where fracture initiated. The site labeled "s" is the same in each photograph. The crack shown in (b) was defined by tracing it with a felt-tip pen.

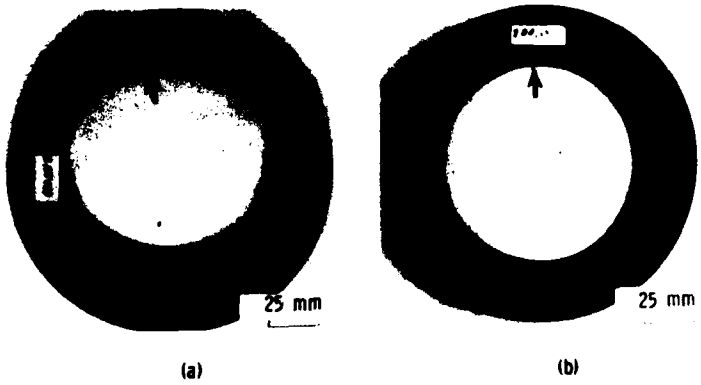

Figure 5. RBSN forward shroud from 10-kW turbo alternator after testing with (a) front view and (b) rear view. Arrow points to location of subcritical crack.

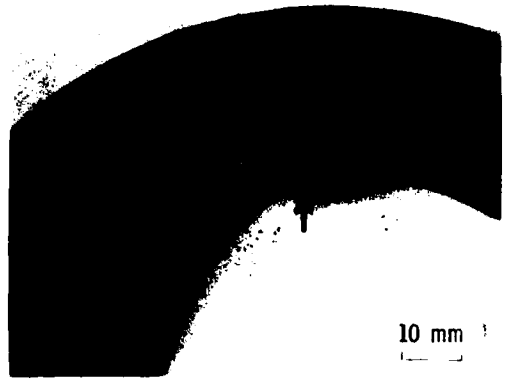

Figure 6. Detail of subcritical crack in forward shroud 1-Df. The crack was defined by tracing it with a felt-tip pen.

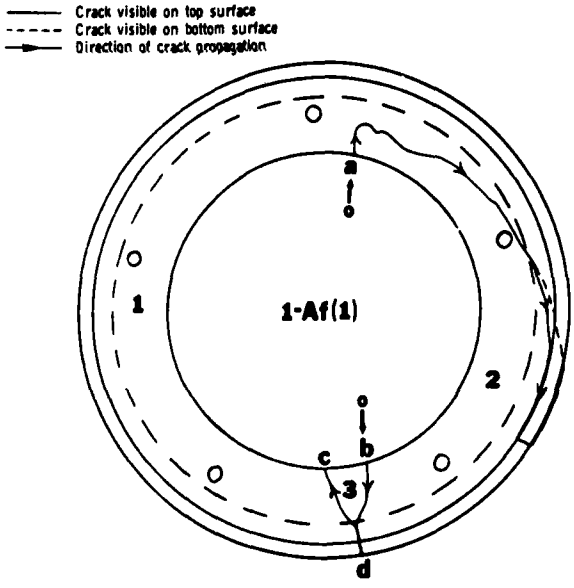

Figure 7. Fracture patterns in RBSN forward shroud after testing. The arrows labeled "o" indicate sites where fracture initiated.

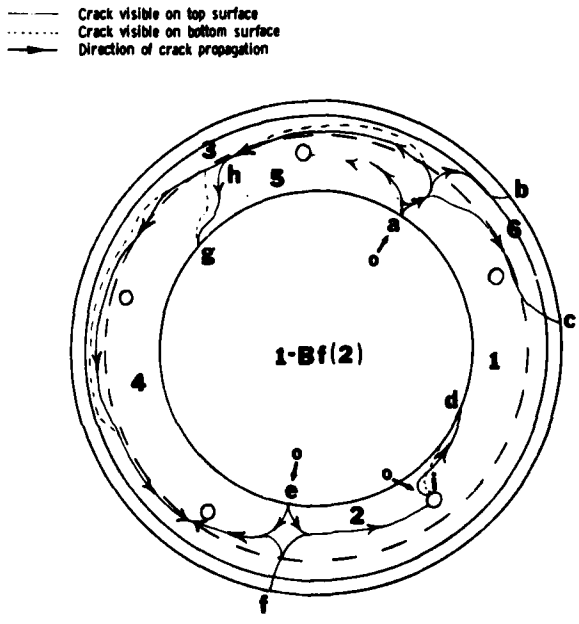

Figure 8. Fracture patterns in RBSN forward shroud after testing. The arrows labeled "o" indicate sites where fracture initiated. Note area near hole (lower left) where circumferential cracks meet.

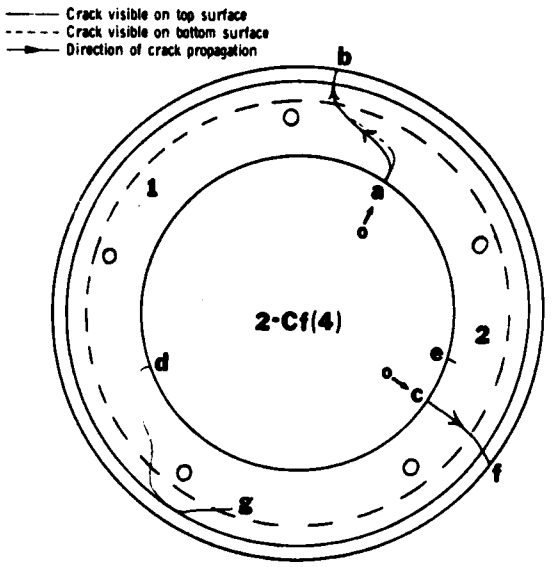

Figure 9. Fracture patterns in RBSN forward shroud after testing. The arrows labeled "o" indicate sites where fracture initiated. The line d-g indicates a subcritical crack.

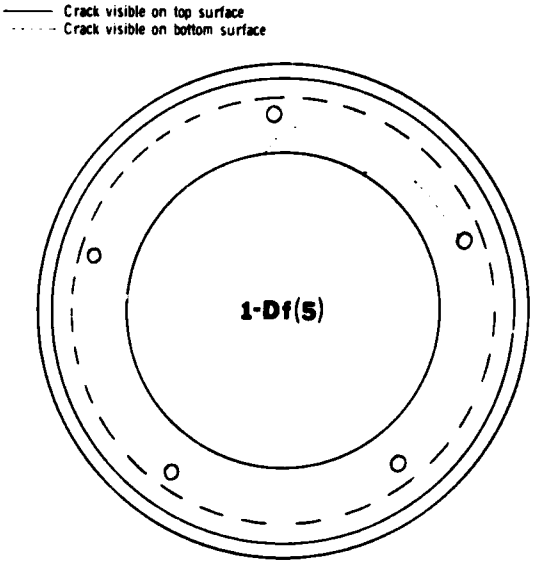

Figure 10. Fracture patterns in RBSN forward shroud after testing. The cracks shown are subcritical.

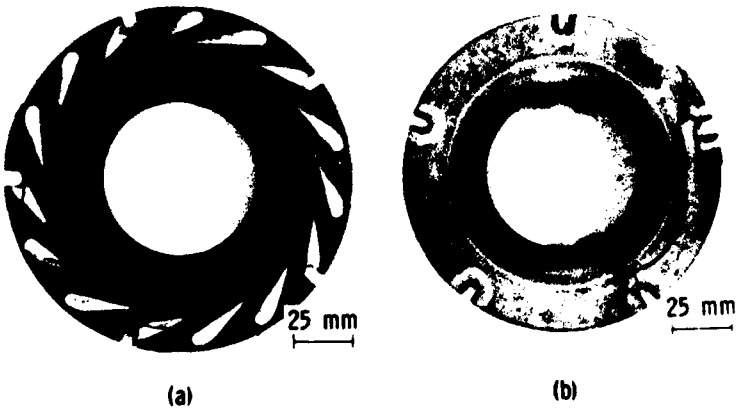

Figure 11. RBSN rear shroud after 50 hours of testing in the 10-kW turbo alternator with (a) front view and (b) rear view. Arrows indicate regions where fracture originated.

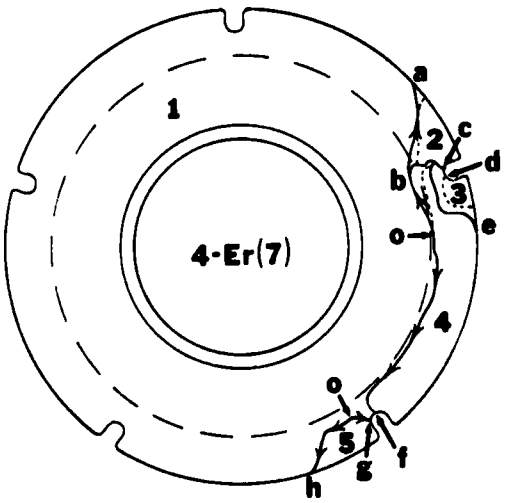

Figure 12. Fracture patterns in RBSN rear shroud after 50 hours of testing. The arrows labeled "o" indicate sites where fracture originated. Crack g-h was present after 33 hours of testing.

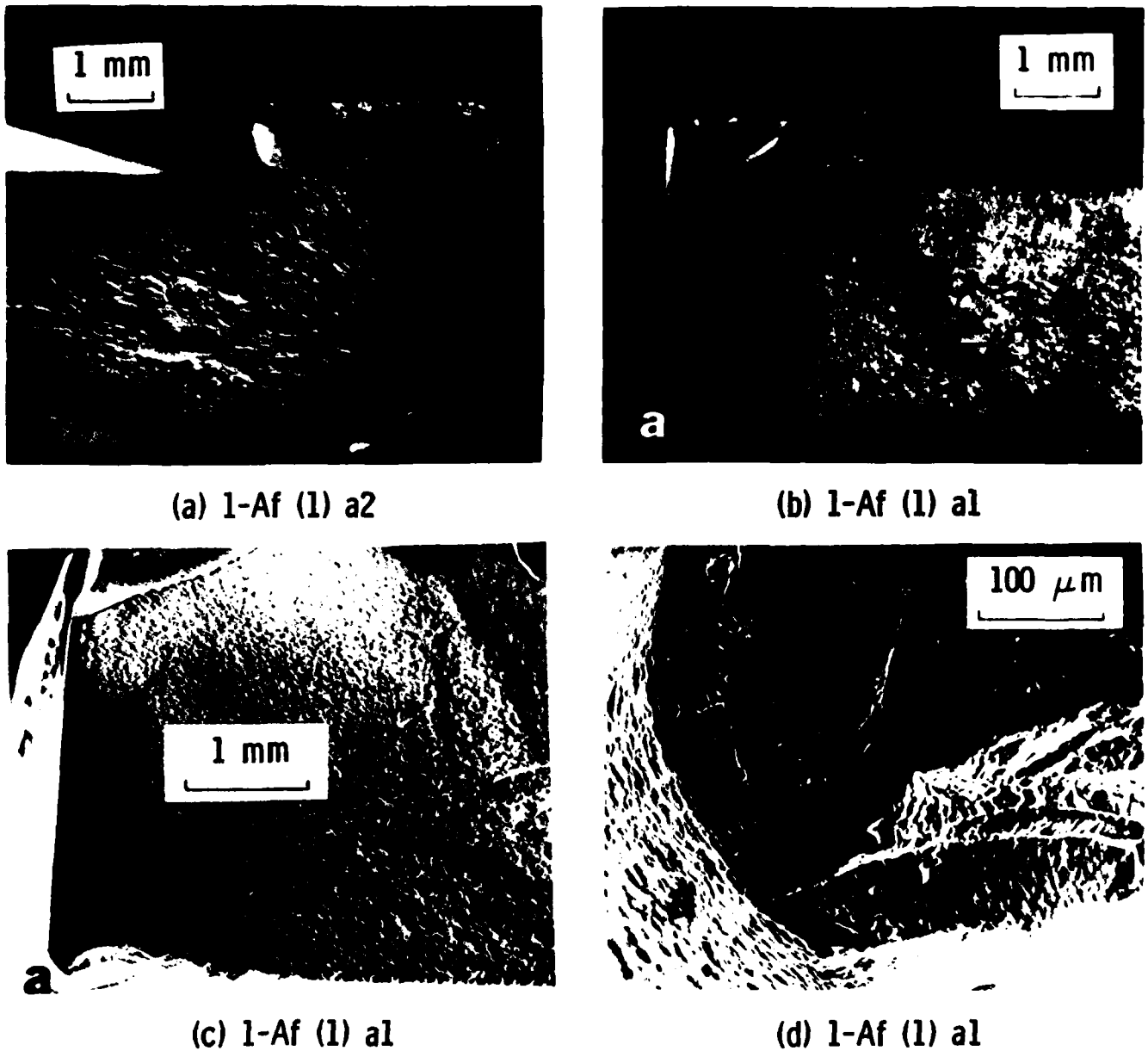

Figure 13. Fracture surfaces near fracture origin "a" in shroud 1-Af (1). (a) and (b) are photomacrographs of matching fracture surfaces; (c) and (d) are scanning electron photomicrographs of surface shown in (b). The prominent surface features in (d) are believed to be cracks emanating from the machining striae evident on the surface (lower left).

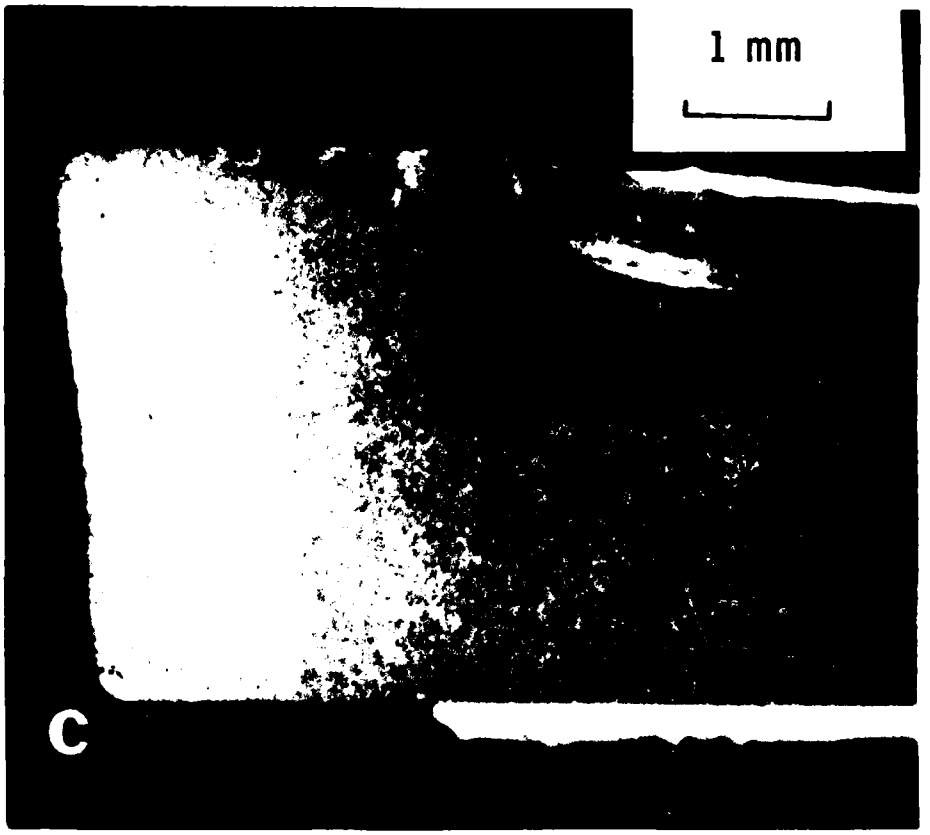

1-Af (1) c3

Figure 14. Photomacrograph of fracture surface near "c" in shroud 1-Af (1). Hackle lines visible at left indicate that the crack emerged in that area.

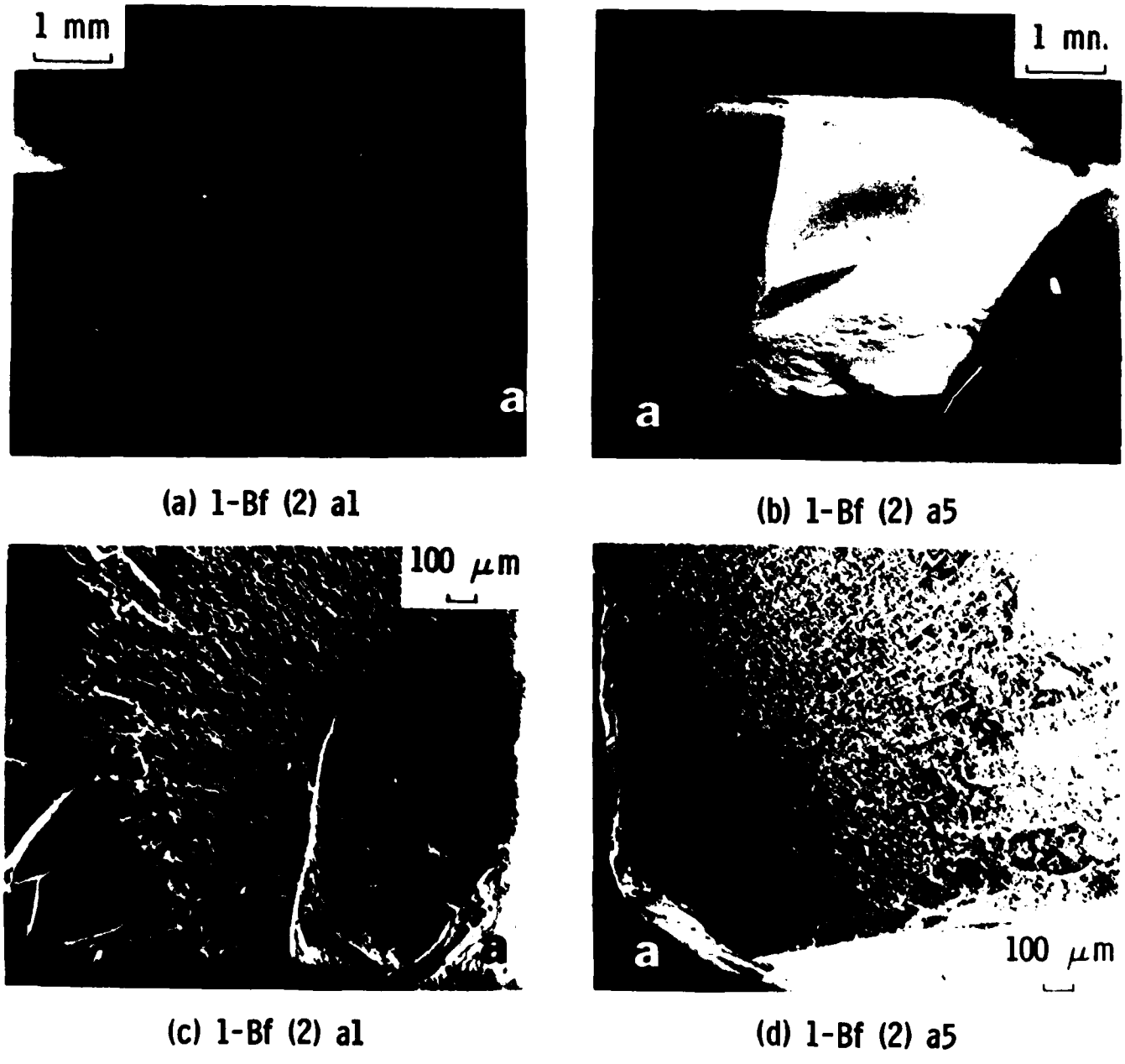

Figure 15. Fracture surfaces near fracture origin "a" in shroud 1-Bf (2). (a) and (b) are photomacrographs of matching fracture surfaces; (c) and (d) are scanning electron photomicrographs of the same surfaces. The chip evident in the lower right of (a) and (c) probably occurred in handling.

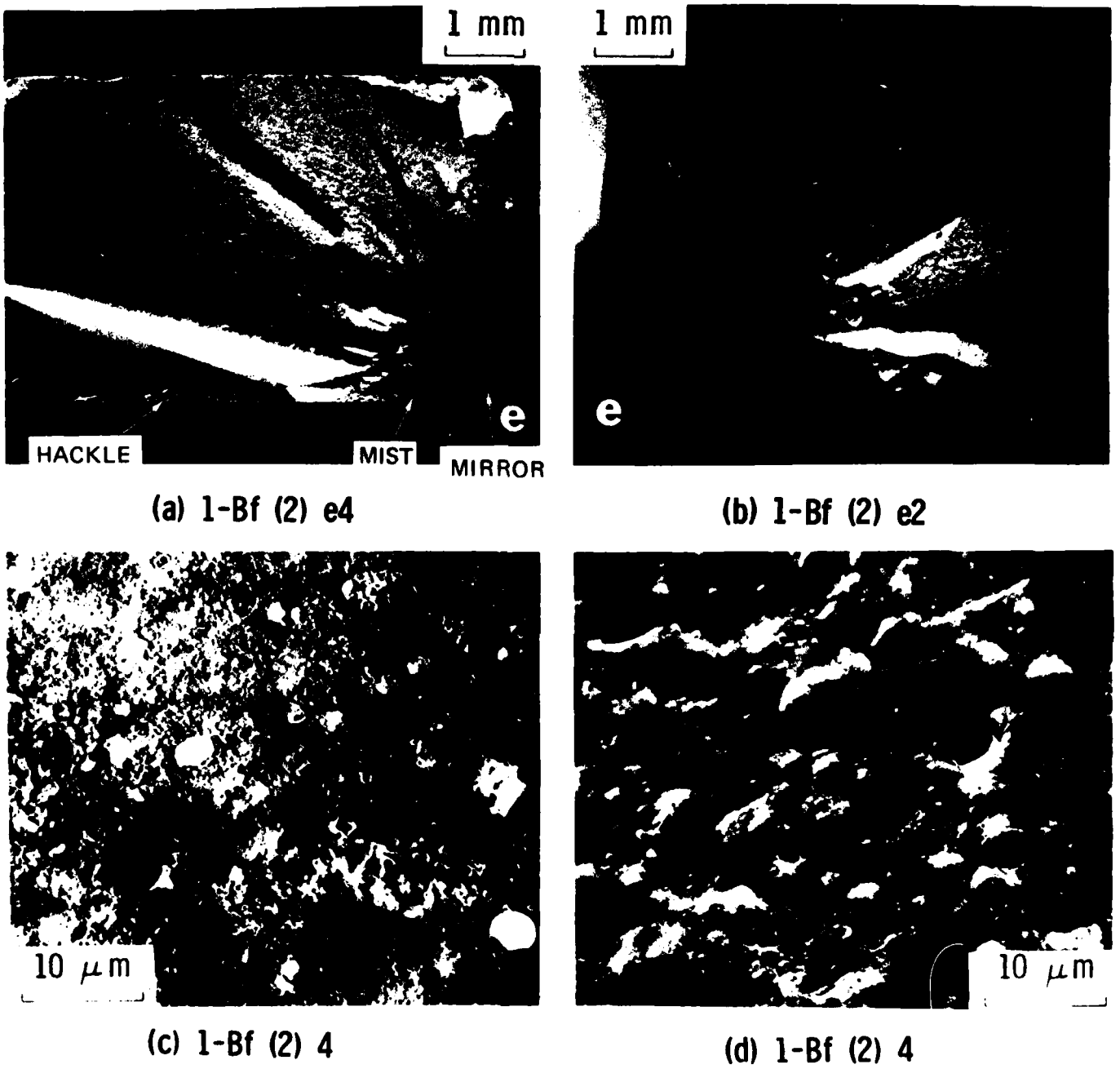

Figure 16. (a) and (b) are photomacrographs of matching fracture surfaces near fracture origin "e" in shroud 1-Bf (2). (c) and (d) are scanning electron photomicrographs showing appearances of surface respectively close to and away from the fracture origin.

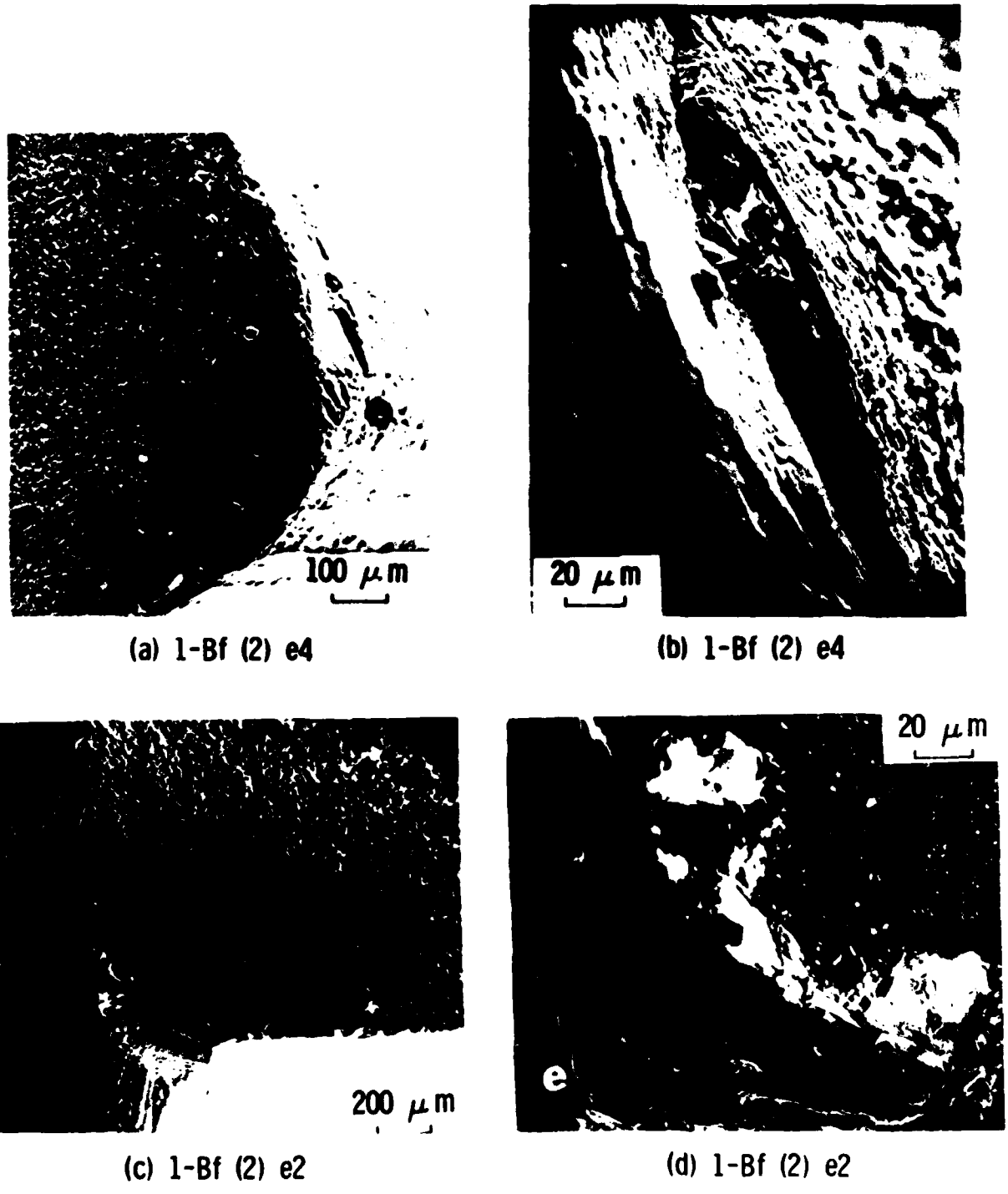

Figure 17. Scanning electron photomicrographs of fracture surfaces near fracture origin "e" in shroud 1-Bf (2). Visible in (a) and (b) are machining striae and a chip near "e". The probable fracture origin, a large pore, is visible in (c) and (d). The white area in (d) are probably dust.

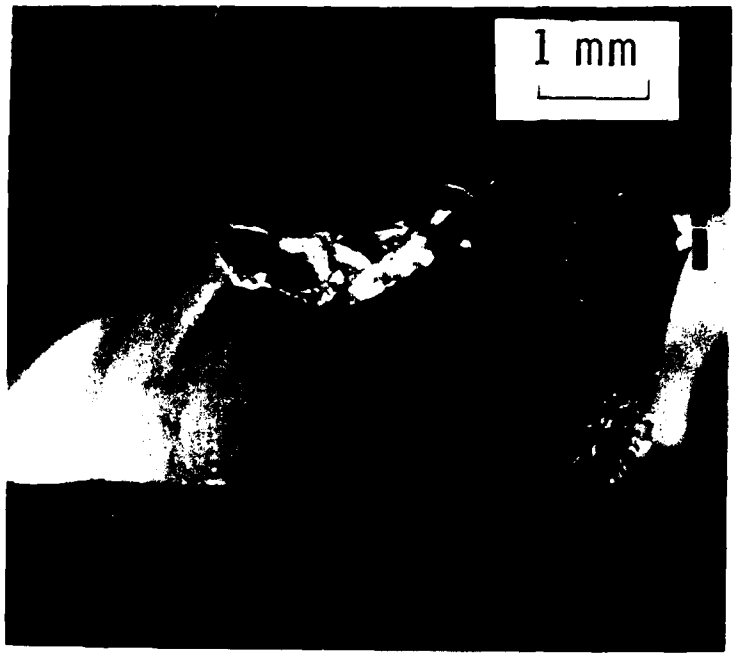

(a) 1-Bf (2) i1

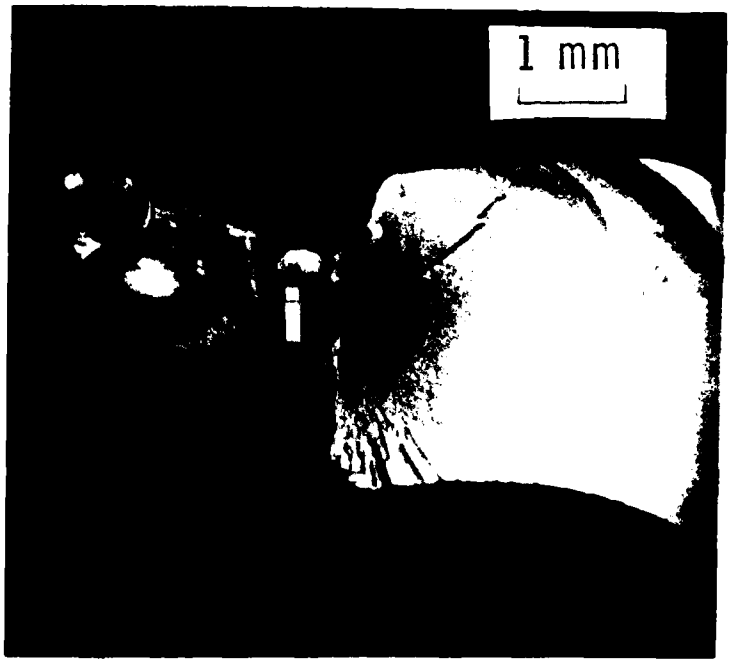

(b) 1-Bf (2) i2

Figure 18. Photomacrographs of matching fracture surfaces near fracture origin "i" in shroud 1-Bf (2).

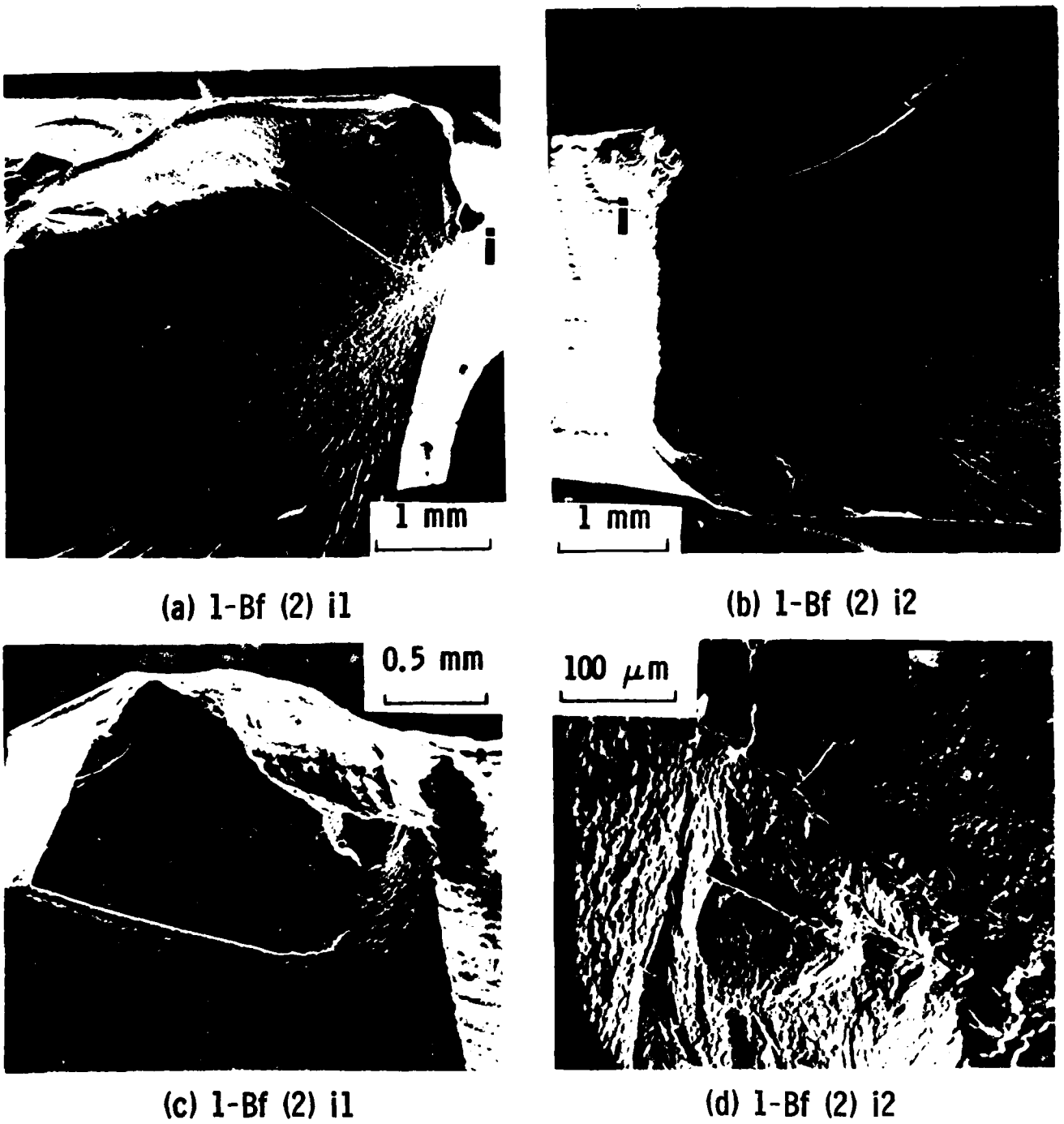

Figure 19. Scanning electron photomicrographs of fracture surfaces near fracture origin "i" in shroud 1-Bf (2).

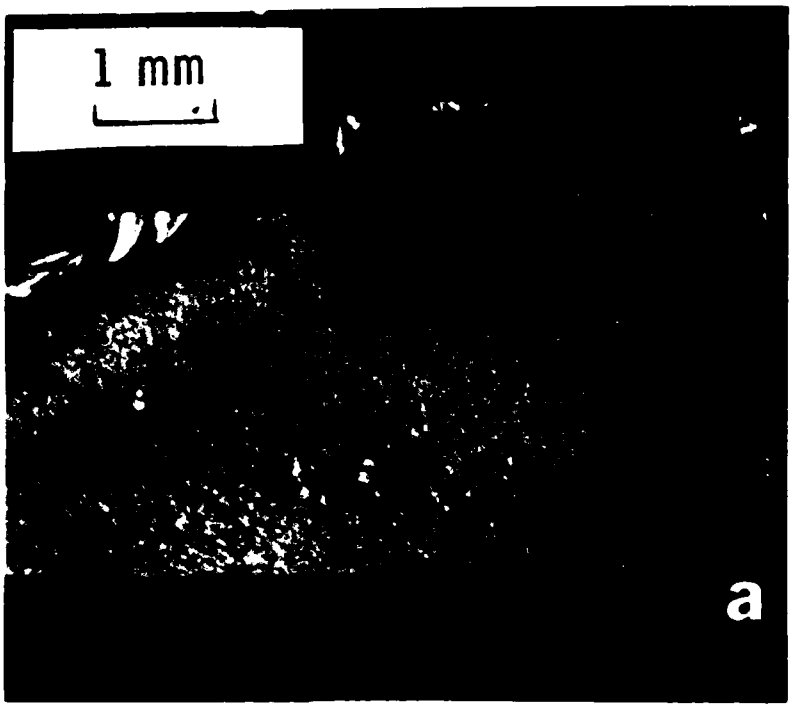

(a) 2-Cf (4) a2

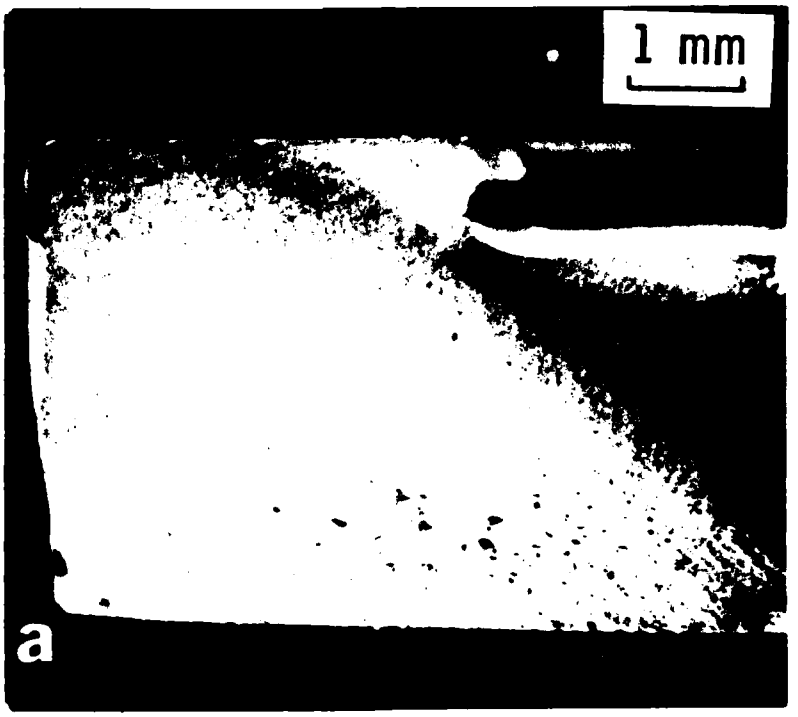

(b) 2-Cf (4) a1

Figure 20. Photomacrographs of matching fracture surfaces near fracture origin "a" in shroud 2-Cf (4).

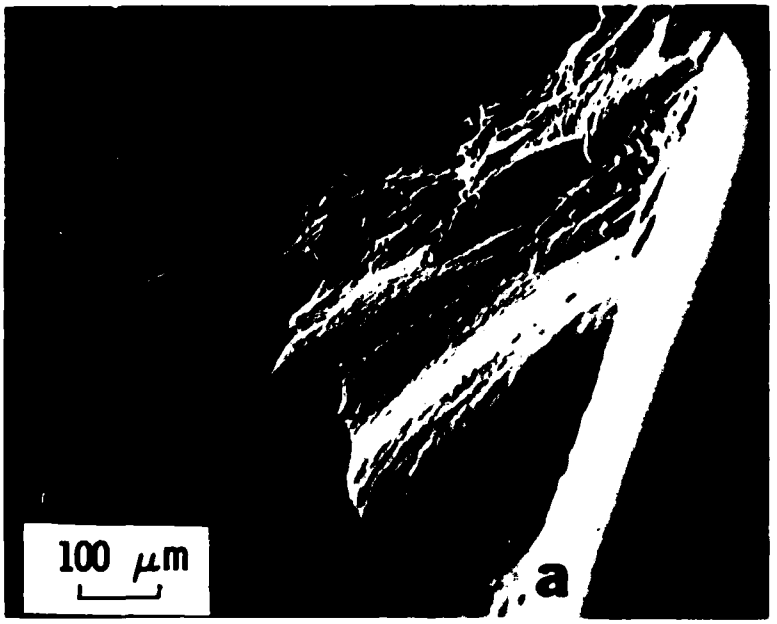

(a) 2-Cf (4) a2

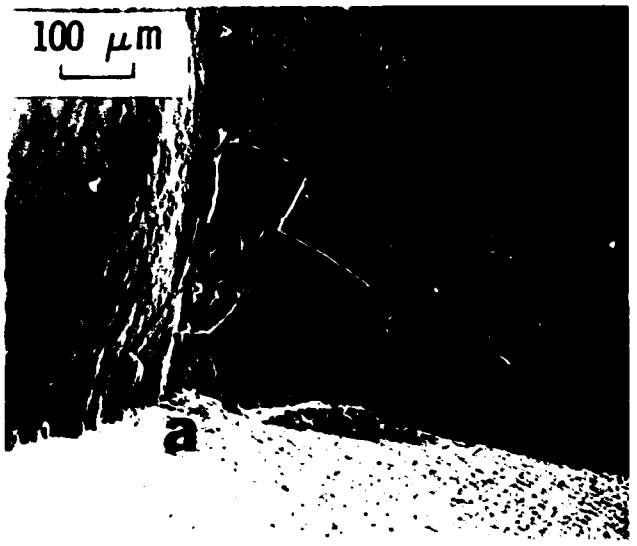

(b) 2-Cf (4) a1

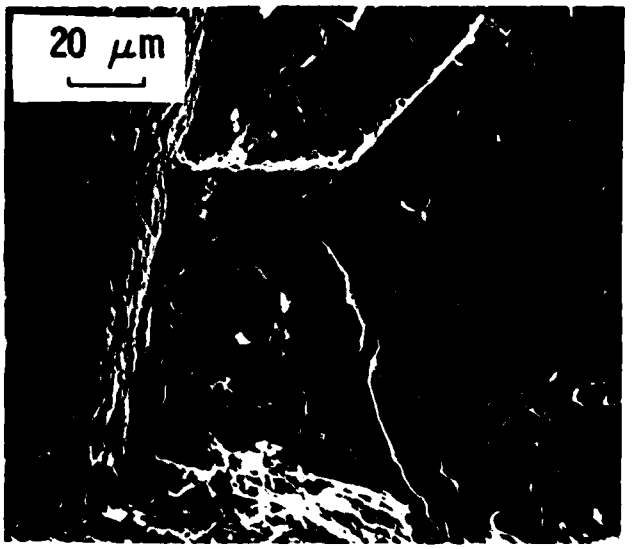

(c) 2-Cf (4) a1

Figure 21. Scanning electron photomicrographs of fracture surfaces near fracture origin "a" in shroud 2-Cf (4). The probable fracture origin is the large inclusion evident near the center of (c).

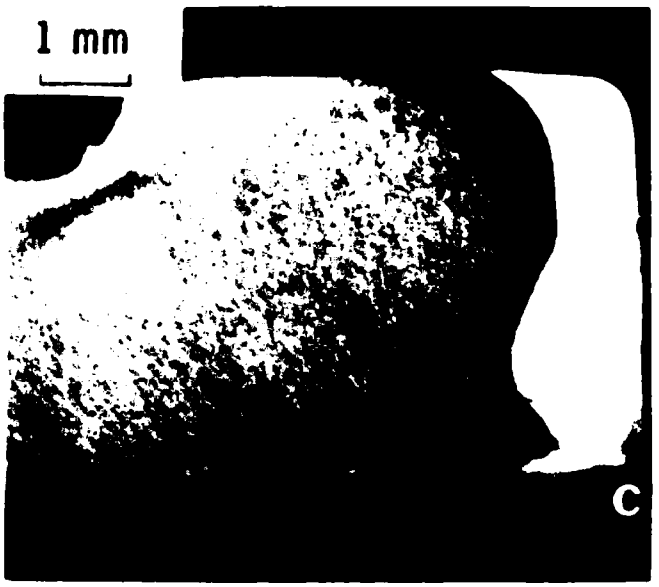

(a) 2-Cf (4) c1

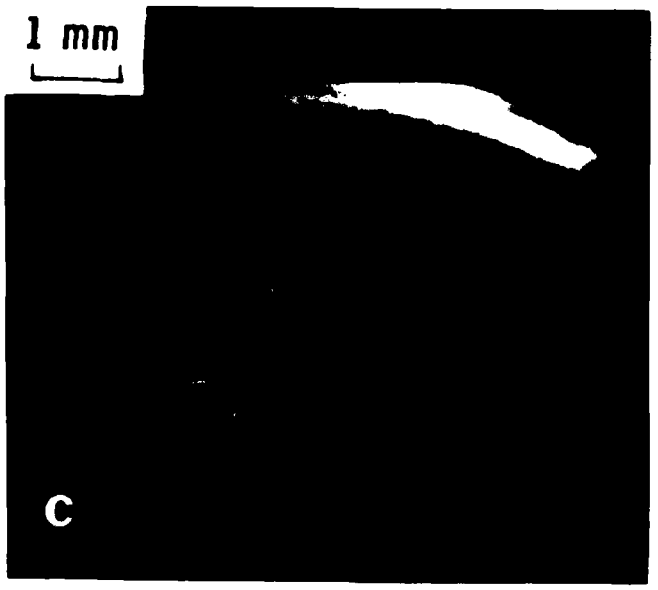

(b) 2-Cf (4) c2

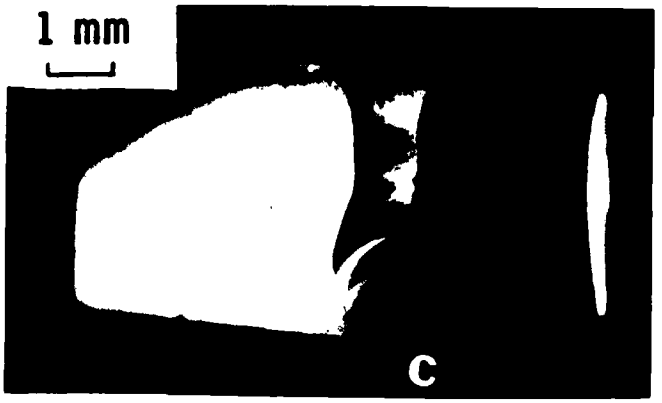

(c) 2-Cf (4) c1

Figure 22. Photomacrographs of matching fracture surfaces near fracture origin "c" in shroud 2-Cf (4). In (c) the specimen was rotated to show more clearly the corner surface visible in (a).

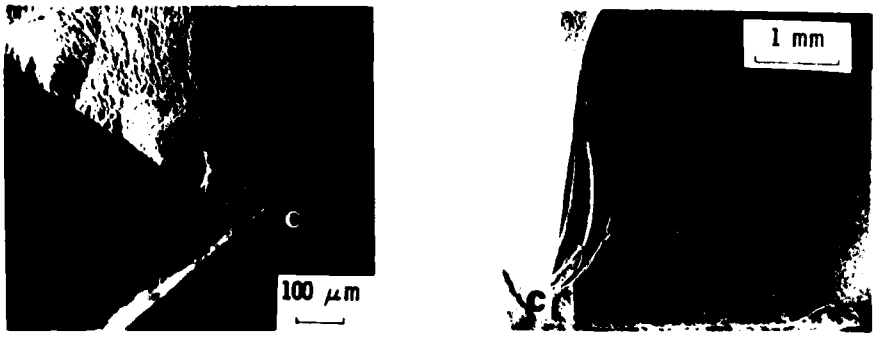

(a) 2-Cf (4) c1 (b) 2-Cf (4) c2

Figure 23. Scanning electron photomicrographs of fracture surfaces near fracture origin "c" in shroud 2-Cf (4).

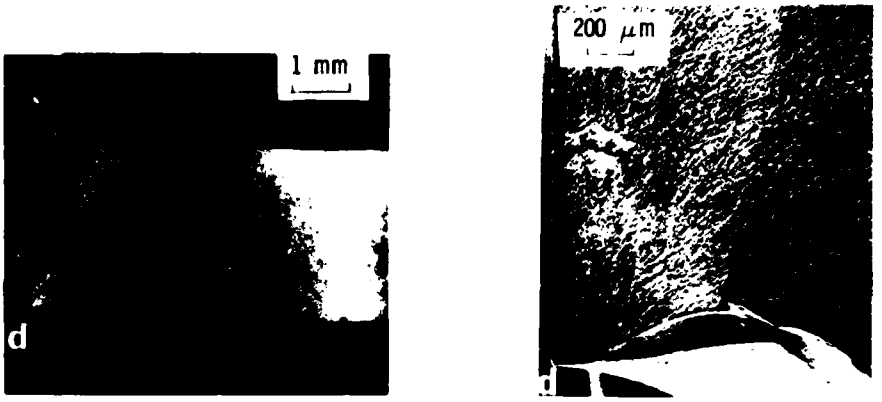

(a) 2-Cf (4) d1 (b) 2-Cf (4) d1

Figure 24. Fracture surfaces near "d" in shroud 2-Cf (4). (a) is a photomacrograph and (b) is a scanning electron photomicrograph.

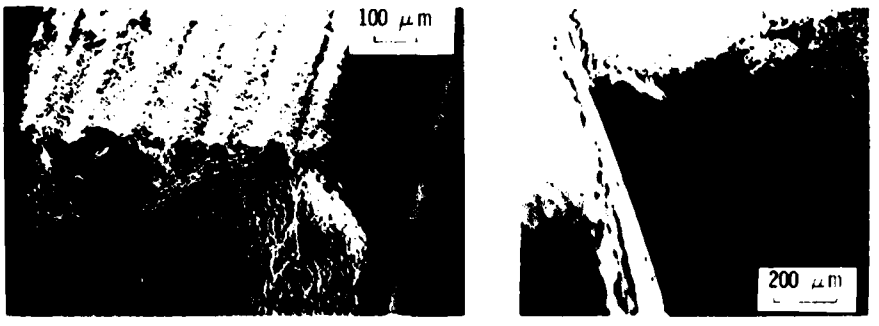

(a) 2-Cf (4) 1 (b) 1-Bf (2) 5

Figure 25. Scanning electron photomicrographs showing machining striations in shrouds.

(a) 4-Er(7) 1 (b) 4-Er(7) 5

Figure 26. Photomacrographs of matching fracture surfaces near "g" in shroud 4-Er (7). This fracture initiated internally.

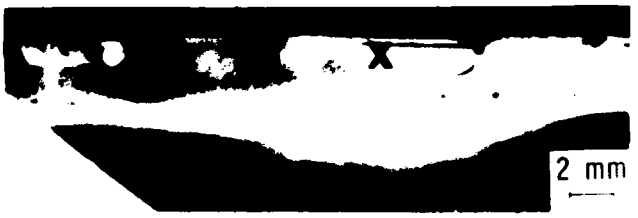

(a) 4-Er(7) 1

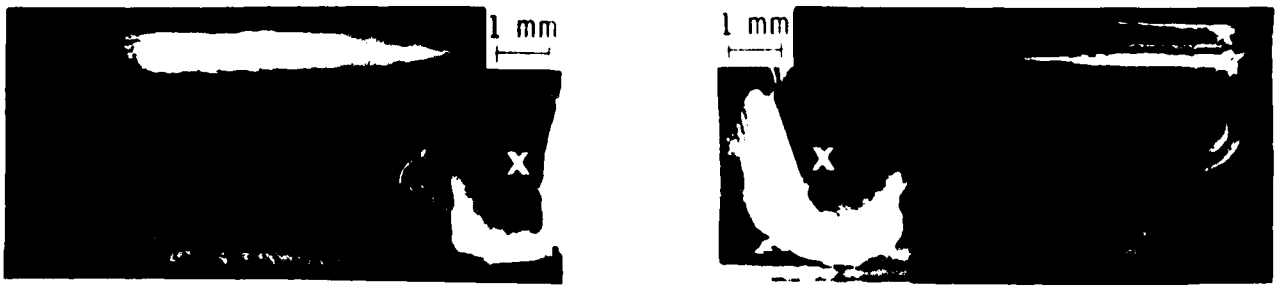

(b) 4-Er(7) 4 (c) 4-Er(7) 1

Figure 27. Fracture surfaces near "b" in shroud 4-Er (7). (a) shows a large area of the fracture surface on piece No. 1; (b) and (c) show matching fracture surfaces on piece No. 4 and 1, respectively. The large chip evident in (c) is not visible in (b), indicating that chipping occurred after fracture of the component.

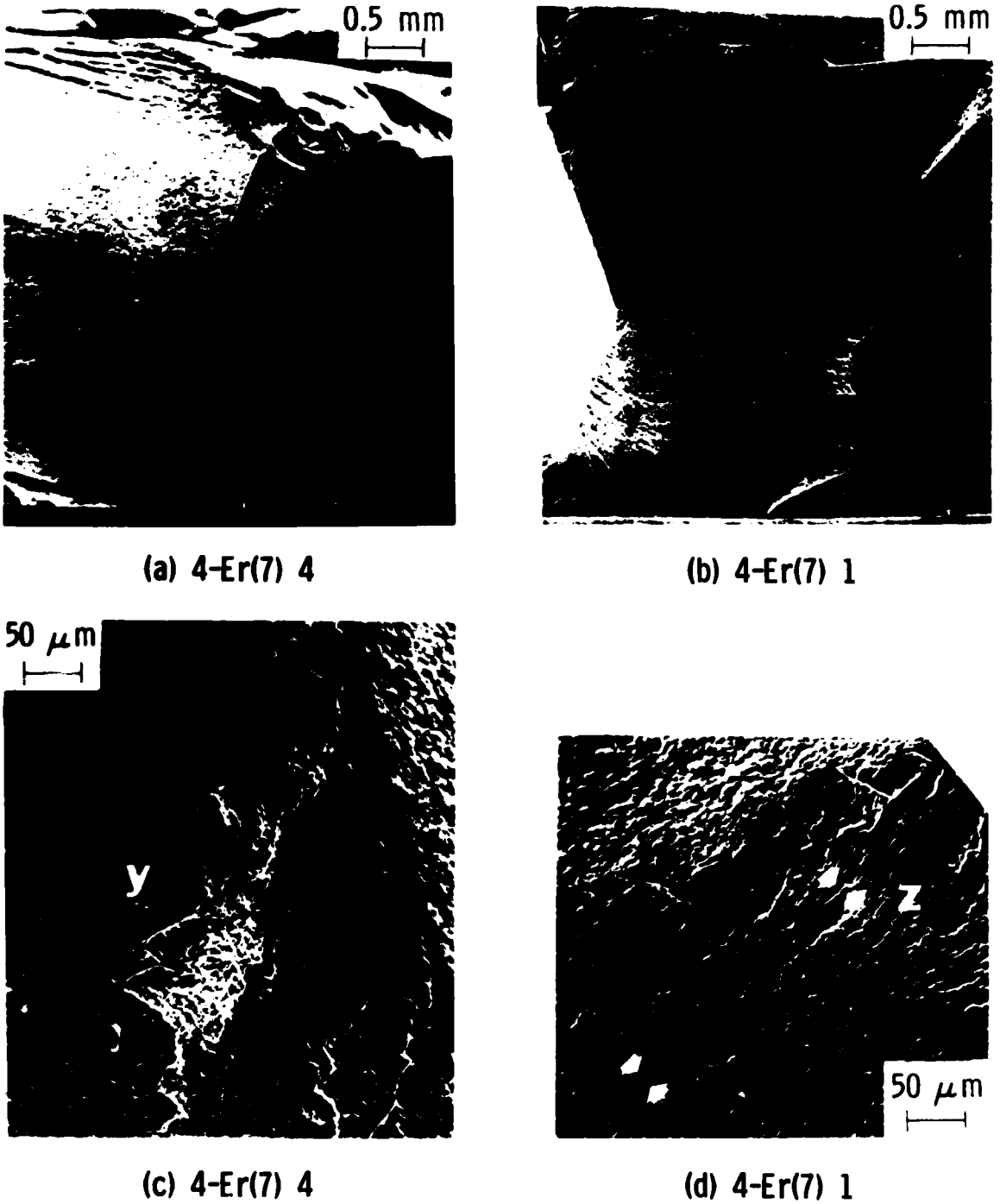

Figure 28. Scanning electron photomicrographs of fracture surfaces near "b" in shroud 4-Er (7). (a) and (b) are matching surfaces; (c) and (d) show details at higher magnification. The porous area near "y" is probably the defect that initiated fracture.

(a) 4-Er(7) 3 (b) 4-Er(7) 3

Figure 29. Possible fracture origin near "d" in shroud 4-Er (7). (b) is a scanning electron photomicrograph of the area indicated by the arrow in (a).

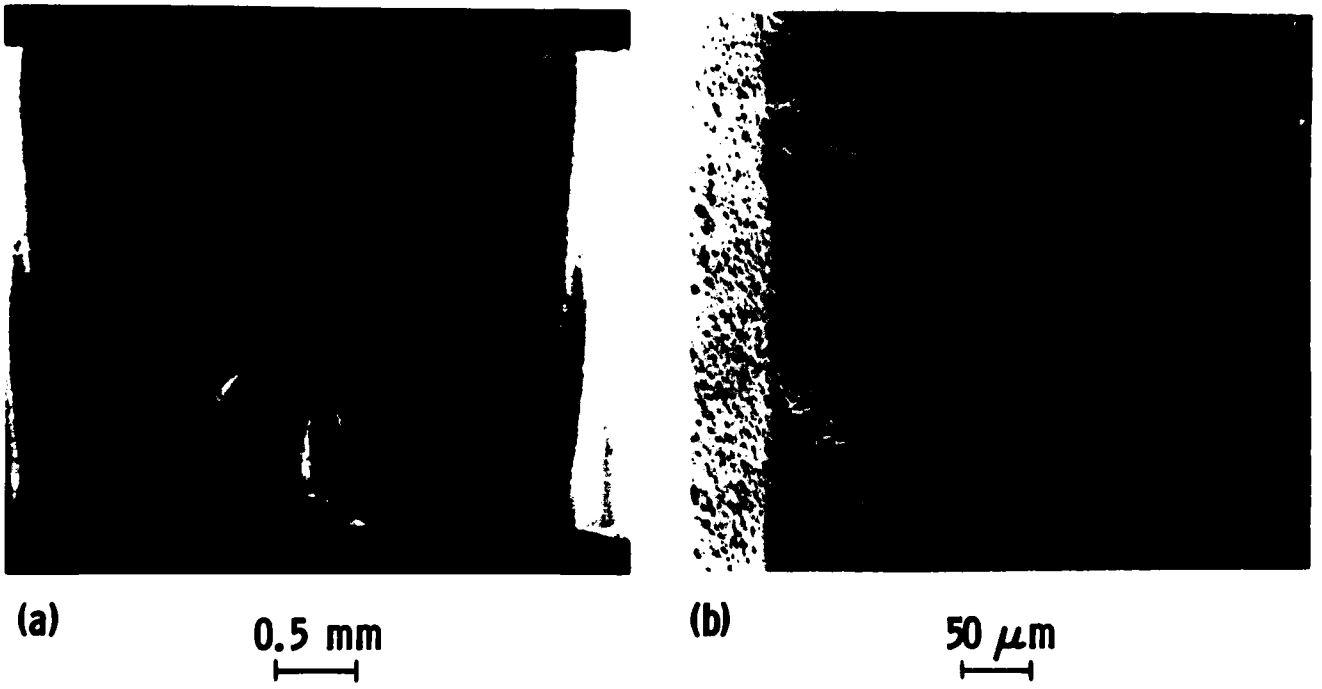

Figure 30. Appearance of bend bar from shroud 1-Af (1) after fracture with (a) matching fracture surfaces and (b) scanning electron photomicrograph of the fracture origin. Failure originated in the porous region ("material defect") shown.

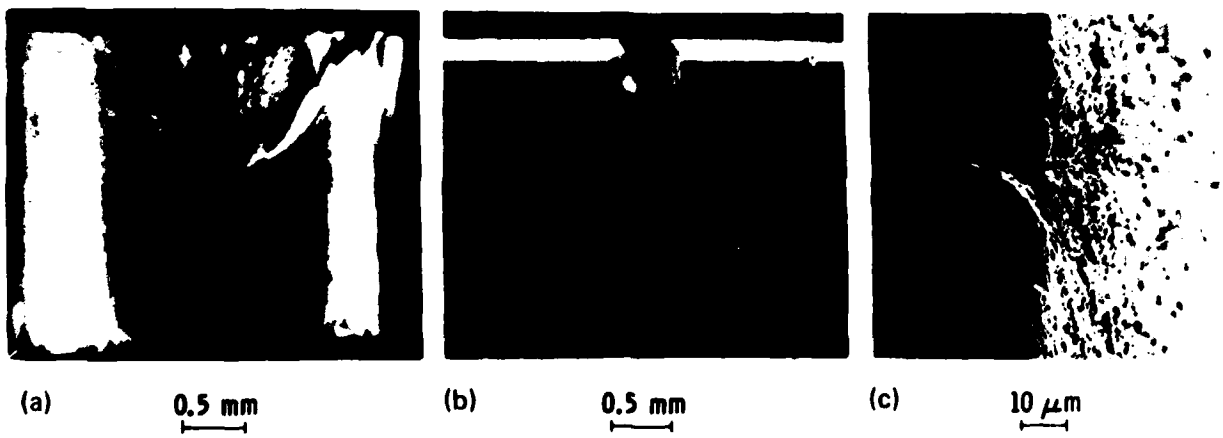

Figure 31. Appearance of bend bar from shroud 1-Bf (2) after fracture. (a) matching fracture surfaces; (b) specimen surface; and (c) scanning electron photomicrograph near fracture origin. This specimen failed from the machining striation indicated by the arrow in (b).

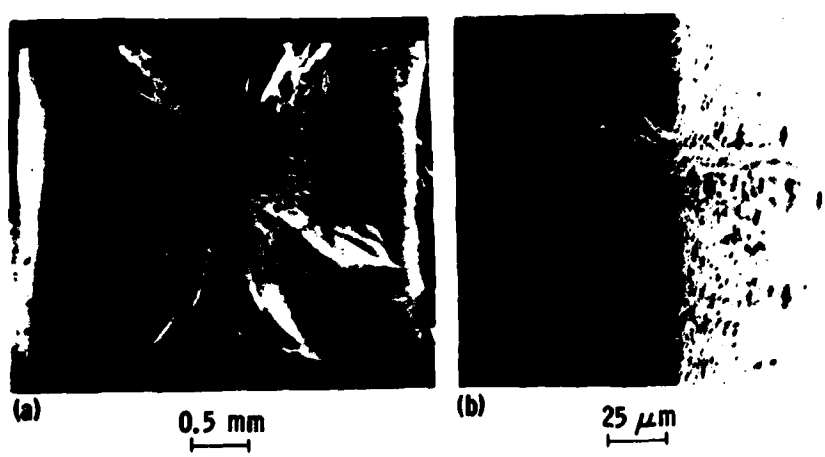

Figure 32. Appearance of bend bar from shroud 1-Af (1) after fracture. (a) Matching fracture surfaces and (b) scanning electron photomicrograph of the fracture origin. This specimen failed from a mixed defect, i.e., a machining striation interacting with porosity as seen in (b).

Figure 33. Matching fracture surfaces of RBSN bend bar from shroud 1-Ar (1). The arrow indicates an internal defect at the fracture origin.

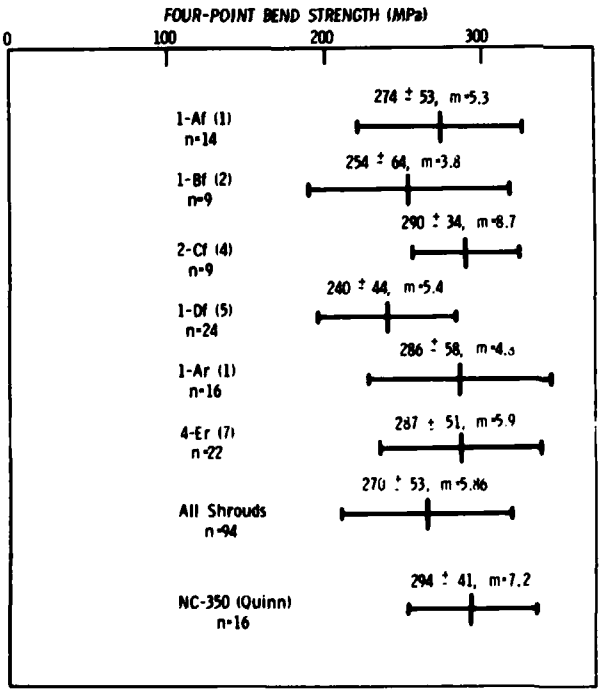

Figure 34. Results of bend tests conducted on specimens machined from RBSN shrouds. The error bars indicate standard deviations.

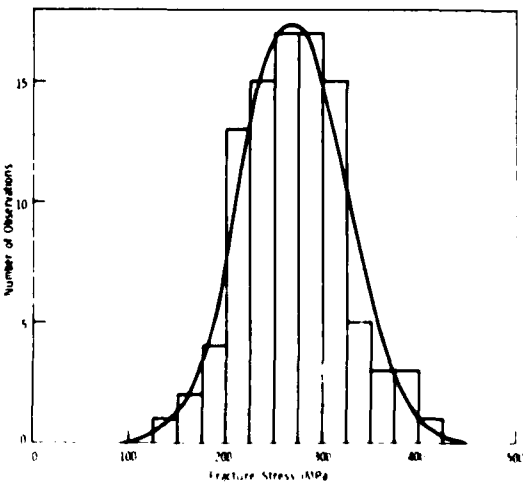

Figure 35. Histogram of bend bar fracture data with normal distribution curve overlay.

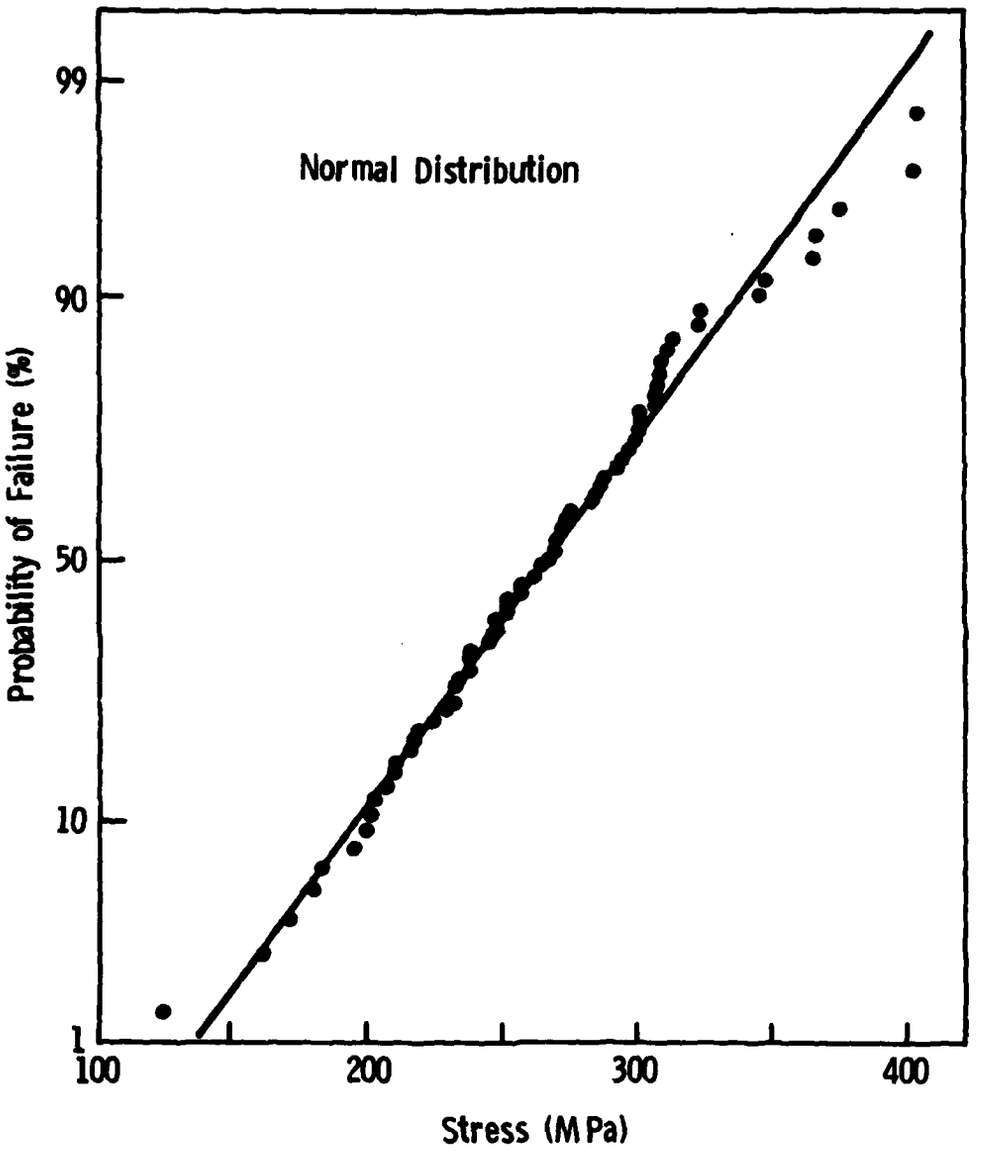

Figure 36. Data from all bend tests plotted according to a normal distribution function.

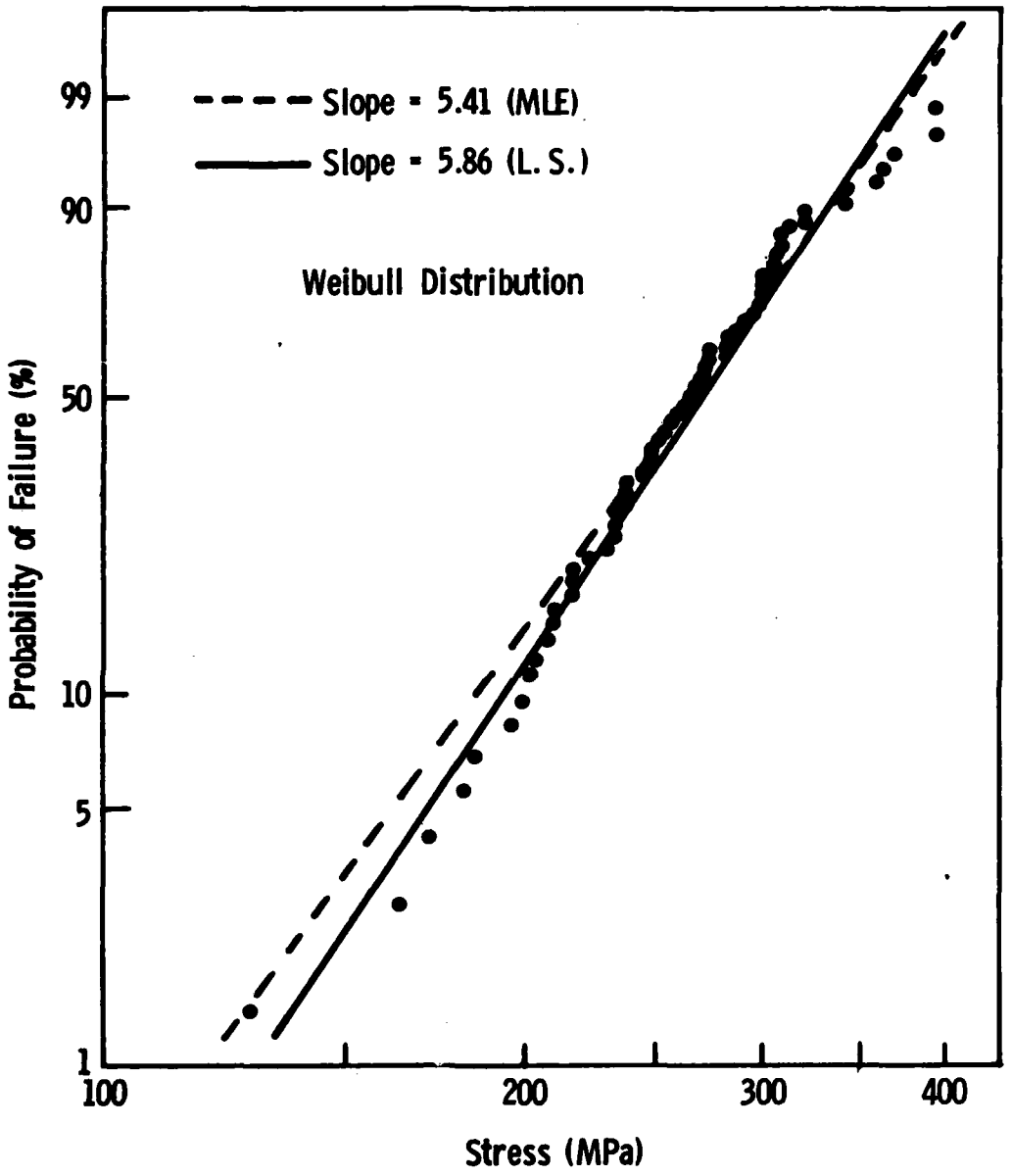

Figure 37. Data from all bend tests plotted according to the Weibull distribution function.

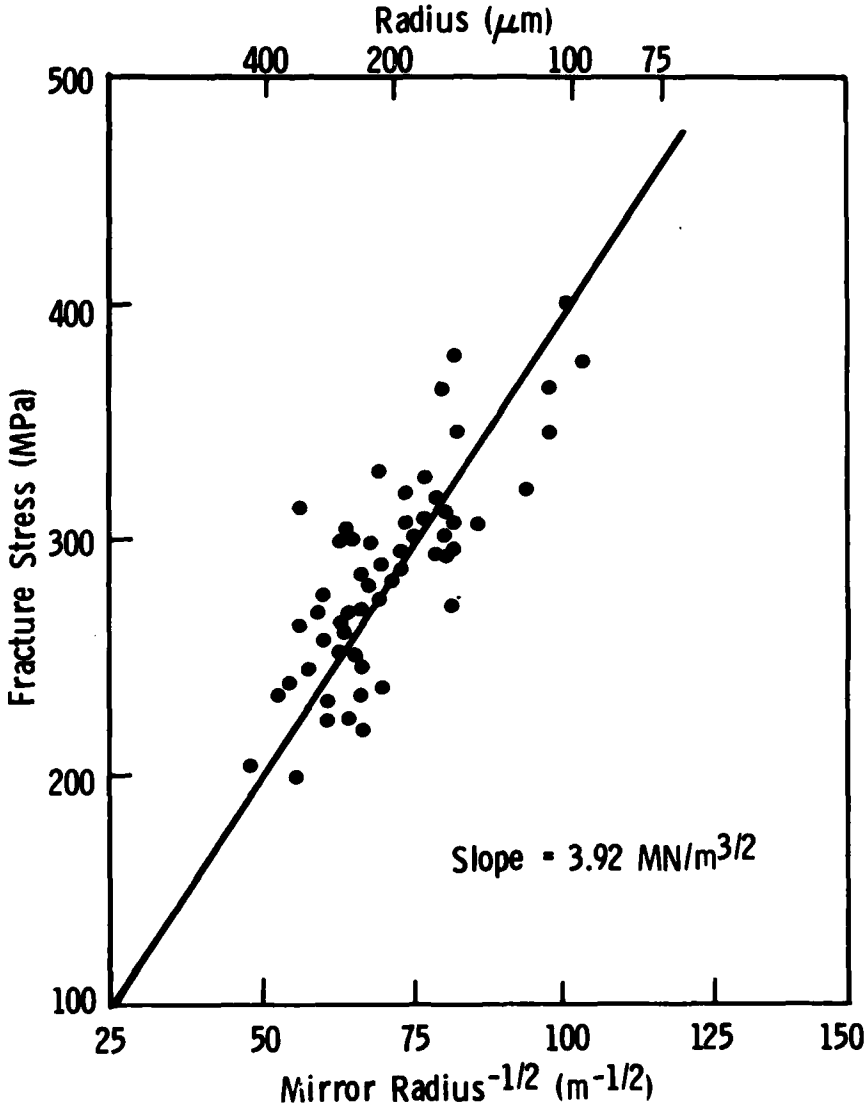

Figure 38. Fracture stress versus fracture mirror radius after Equation 1. All data are from bend specimens.

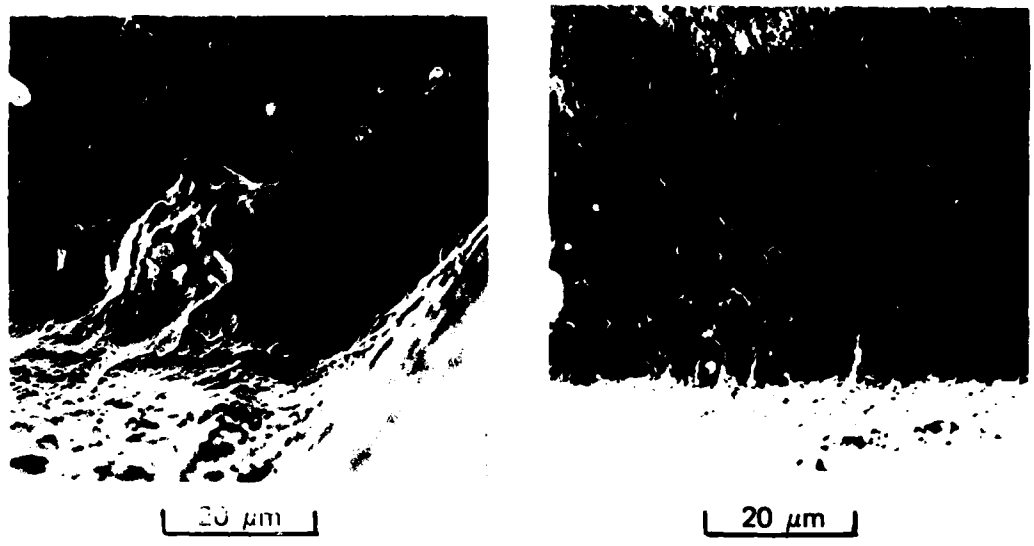

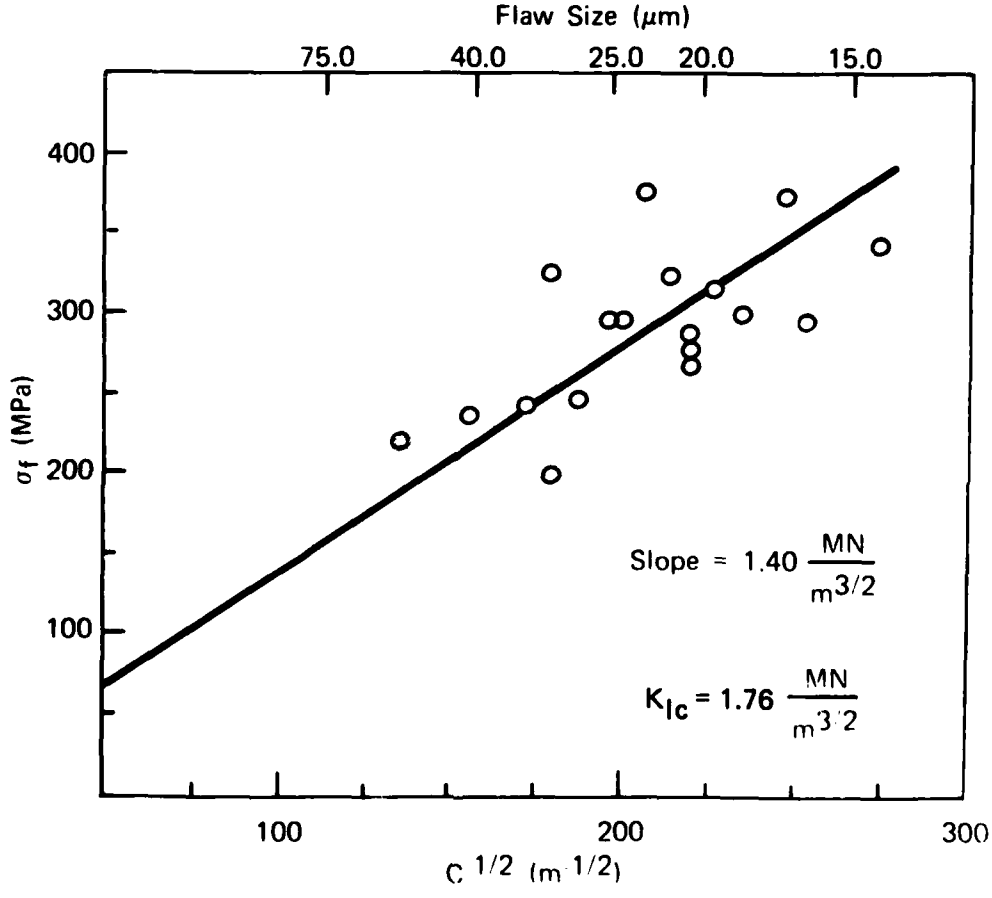

Figure 39. Fracture stress versus flaw size after Equation 2. Insert shows typical flaws.

DISTRIBUTION LIST

No. of Copies	To
	Office of the Under Secretary of Defense for Research and Engineering, The Pentagon, Washington, DC 20301
1	ATTN: Mr. J. Persh
1	Dr. G. Gamota
12	Commander, Defense Technical Information Center, Cameron Station, Building 5, 5010 Duke Street, Alexandria, VA 22314
1	National Technical Information Service, 5285 Port Royal Road, Springfield, VA 22161
	Director, Defense Advanced Research Projects Agency, 1400 Wilson Boulevard, Arlington, VA 22209
1	ATTN: Dr. A. Bement
1	Dr. Van Reuth
1	MAJ Harry Winsor
	Battelle Columbus Laboratories, Metals and Ceramics Information Center, 505 King Avenue, Columbus, OH 43201
1	ATTN: Mr. Winston Duckworth
1	Dr. D. Niesz
1	Dr. R. Wills
	Deputy Chief of Staff, Research, Development, and Acquisition, Headquarters, Department of the Army, Washington, DC 20301
1	ATTN: DAMA-ARZ
1	DAMA-CSS, Dr. J. Bryant
1	DAMA-PPP, Mr. R. Vawter
	Commander, U.S. Army Medical Research and Development Command, Fort Detrick, Frederick, MD 21701
1	ATTN: SGRD-SI, Mr. Lawrence L. Ware, Jr.
	Commander, Army Research Office, P.O. Box 12211, Research Triangle Park, NC 27709
1	ATTN: Information Processing Office
1	Dr. G. Mayer
1	Dr. J. Hurt
	Commander, U.S. Army Materiel Development and Readiness Command, 5001 Eisenhower Avenue, Alexandria, VA 22333
1	ATTN: DRCDMD-ST
1	DRCLDC
	Commander, U.S. Army Electronics Research and Development Command, Fort Monmouth, NJ 07703
1	ATTN: DELSD-L
	Commander, U.S. Army Materiel Systems Analysis Activity, Aberdeen Proving Ground, MD 21005
1	ATTN: DRXSY-MP, H. Cohen
	Commander, U.S. Army Night Vision Electro-Optics Laboratory, Fort Belvoir, VA 22060
1	ATTN: DELNV-S, Mr. P. Travesky
1	DELNV-L-D, Dr. R. Buser
	Commander, Harry Diamond Laboratories, 2800 Powder Mill Road, Adelphi, MD 20783
1	ATTN: Mr. A. Benderly
1	Technical Information Office
1	DELHD-RAE
	Commander, U.S. Army Missile Command, Redstone Arsenal, AL 35809
1	ATTN: Mr. P. Ormsby
1	Technical Library
1	DRSMI-TB, Redstone Scientific Information Center
	Commander, U.S. Army Aviation Research and Development Command, 4300 Goodfellow Boulevard, St. Louis, MO 63120
1	ATTN: DRDAV-EGX
1	DRDAV-QF
1	Technical Library
	Commander, U.S. Army Natick Research and Development Laboratories, Natick, MA 01760
1	ATTN: Technical Library
1	Dr. J. Hanson
	Commander, U.S. Army Satellite Communications Agency, Fort Monmouth, NJ 07703
1	ATTN: Technical Document Center
	Commander, U.S. Army Tank-Automotive Command, Warren, MI 48090
1	ATTN: Dr. W. Bryzik
1	Mr. E. Hamperian
1	D. Rose
1	DRSTA-RKA
1	DRSTA-UL, Technical Library
1	DRSTA-R
	Commander, U.S. Army Armament Research and Development Command, Dover, NJ 07801
1	ATTN: Mr. J. Lannon
1	Dr. G. Vezzoli
1	Mr. A. Graf
1	Mr. Harry E. Pebly, Jr., PLASTEC, Director
1	Technical Library
	Commander, U.S. Army Armament Materiel Readiness Command, Rock Island, IL 61299
1	ATTN: Technical Library
	Commander, Aberdeen Proving Ground, MD 21005
1	ATTN: DRDAR-CLB-PS, Mr. J. Vervier
	Commander, U.S. Army Mobility Equipment Research and Development Command, Fort Belvoir, VA 22060
1	ATTN: DRDME-EM, Mr. W. McGovern
1	DRDME-V, Mr. E. York
1	DRDME-X, Mr. H. J. Peters
	Director, U.S. Army Ballistic Research Laboratory, Aberdeen Proving Ground, MD 21005
1	ATTN: DRDAR-TSB-S (STINFO)
	Commander, Rock Island Arsenal, Rock Island, IL 61299
1	ATTN: SARRI-EN
	Commander, U.S. Army Test and Evaluation Command, Aberdeen Proving Ground, MD 21005
1	ATTN: DRSTE-ME
	Commander, U.S. Army Foreign Science and Technology Center, 220 7th Street, N.E., Charlottesville, VA 22901
1	ATTN: Military Tech, Mr. W. Marley
	Chief, Benet Weapons Laboratory, LCWSL, USA ARRADCOM, Watervliet, NY 12189
1	ATTN: DRDAR-LCB-TL
	Commander, Watervliet Arsenal, Watervliet, NY 12189
1	ATTN: Dr. T. Davidson
	Director, Eustis Directorate, U.S. Army Mobility Research and Development Laboratory, Fort Eustis, VA 23604
1	ATTN: Mr. J. Robinson, DAVDL-E-MOS (AVRADCOM)
1	Mr. C. Walker
	Commander, U.S. Army Engineer Waterways Experiment Station, Vicksburg, MS 39180
1	ATTN: Research Center Library
	Chief of Naval Research, Arlington, VA 22217
1	ATTN: Code 471
1	Dr. A. Diness
1	Dr. R. Pohanka
	Naval Research Laboratory, Washington, DC 20375
1	ATTN: Dr. J. M. Krafft - Code 5830
1	Mr. R. Rice
1	Dr. Jim C. I. Chang
	Headquarters, Naval Air Systems Command, Washington, DC 20360
1	ATTN: Code 5203
1	Code MAT-042M
1	Mr. I. Macklin
	Headquarters, Naval Sea Systems Command, 1941 Jefferson Davis Highway, Arlington, VA 22376
1	ATTN: Code 035
	Headquarters, Naval Electronics Systems Command, Washington, DC 20360
1	ATTN: Code 504

No. of Copies	To
	Commander, Naval Weapons Center, China Lake, CA 93555
1	ATTN: Mr. F. Markarian
1	Mr. E. Teppo
1	Mr. M. Ritchie
	Commander, U.S. Air Force of Scientific Research, Building 410, Bolling Air Force Base, Washington, DC 20332
1	ATTN: MAJ W. Simmons
	Commander, U.S. Air Force Wright Aeronautical Laboratories, Wright-Patterson Air Force Base, OH 45433
1	ATTN: AFWAL/MLLM, Dr. N. Tallan
1	AFWAL/MLLM, Dr. H. Graham
1	AFWAL/MLLM, Dr. R. Ruh
1	AFWAL/MLLM, Dr. A. Katz
1	AFWAL/MLLM, Mr. K. S. Mazdiyasni
1	Aero Propulsion Labs, Mr. R. Marsh
	Commander, Air Force Weapons Laboratory, Kirtland Air Force Base, Albuquerque, NM 87115
1	ATTN: Dr. R. Rudder
	Commander, Air Force Armament Center, Eglin Air Force Base, FL 32542
1	ATTN: Technical Library
	National Aeronautics and Space Administration, Washington, DC 20546
1	ATTN: Mr. G. C. Deutsch - Code RW
1	Mr. J. Gangler
1	AFSS-AD, Office of Scientific and Technical Information
	National Aeronautics and Space Administration, Lewis Research Center, 21000 Brookpark Road, Cleveland, OH 44135
1	ATTN: J. Accurio, USAMRDL
1	Dr. H. B. Probst, MS 49-1
1	Dr. R. Ashbrook
1	Dr. S. Dutta
1	Mr. S. Grisaffe
	National Aeronautics and Space Administration, Langley Research Center, Center, Hampton, VA 23665
1	ATTN: Mr. J. Buckley, Mail Stop 387
	Commander, White Sands Missile Range, Electronic Warfare Laboratory, OMEW, ERADCOM, White Sands, NM 88002
1	ATTN: Mr. Thomas Reader, DRSEL-WLM-ME
	Department of Energy, Division of Transportation, 20 Massachusetts Avenue, N.W., Washington, DC 20545
1	ATTN: Mr. George Thur (TEC)
1	Mr. Robert Schulz (TEC)
1	Mr. John Neal (CLNRT)
1	Mr. Steve Wander (Fossil Fuels)
	Department of Transportation, 400 Seventh Street, S.W., Washington, DC 20590
1	ATTN: Mr. M. Lauriente
1	Mechanical Properties Data Center, Belfour Stulen Inc., 13917 W. Bay Shore Drive, Traverse City, MI 49684
	National Bureau of Standards, Washington, DC 20234
1	ATTN: Dr. S. Wiederhorn
1	Dr. J. B. Wachtman
	National Research Council, National Materials Advisory Board, 2101 Constitution Avenue, Washington, DC 20418
1	ATTN: D. Groves
1	R. M. Spriggs
	National Science Foundation, Washington, DC 20550
1	ATTN: B. A. Wilcox
	Admiralty Materials Technology Establishment, Polle, Dorset BH16 6JU, UK
1	ATTN: Dr. D. Godfrey
1	Dr. M. Lindley
	AiResearch Manufacturing Company, AiResearch Casting Company, 2525 West 190th Street, Torrance, CA 90505
1	ATTN: Mr. K. Styhr
1	Dr. D. Kotchick

No. of Copies	To
	AiResearch Manufacturing Company, Materials Engineering Dept., 111 South 34th Street, P.O. Box 5217, Phoenix, AZ 85010
1	ATTN: Mr. D. W. Richerson, MS 93-393/503-44
1	Dr. W. Carruthers
	AVCO Corporation, Applied Technology Division, Lowell Industrial Park, Lowell, MA 01887
1	ATTN: Dr. T. Vasilos
	Carborundum Company, Research and Development Division, P.O. Box 1054, Niagara Falls, NY 14302
1	ATTN: Dr. J. A. Coppola
	Case Western Reserve University, Department of Metallurgy, Cleveland, OH 44106
1	ATTN: Prof. A. H. Heuer
	Ceradyne, Inc., P.O. Box 11030, 3030 South Red Hill Avenue, Santa Ana, CA 92705
1	ATTN: Dr. Richard Palicka
	Combustion Engineering, Inc., 911 West Main Street, Chattanooga, TN 37402
1	ATTN: C. H. Sump
	Cummins Engine Company, Columbus, IN 47201
1	ATTN: Mr. R. Kamo
	Defence Research Establishment Pacific, FMO, Victoria, B.C., VOS IBO, Canada
1	ATTN: R. D. Barer
	Deposits and Composites, Inc., 1821 Michael Faraday Drive, Reston, VA 22090
1	ATTN: Mr. R. E. Engdahl
	Electric Power Research Institute, P.O. Box 10412, 3412 Hillview Avenue, Palo Alto, CA 94304
1	ATTN: Dr. A. Cohn
	European Research Office, 223 Old Maryleborne Road, London, NW1 - 5the, England
1	ATTN: Dr. R. Quattrone
1	LT COL James Kennedy
	Ford Motor Company, Turbine Research Department, 20000 Rotunda Drive, Dearborn, MI 48121
1	ATTN: Mr. A. F. McLean
1	Mr. E. A. Fisher
1	Mr. J. A. Mangels
1	Mr. R. Govila
	General Atomic Company, P.O. Box 81608, San Diego, CA 92138
1	ATTN: Jim Halzgraf
	General Electric Company, Mail Drop H-99, Cincinnati, OH 45215
1	ATTN: Mr. Warren Nelson
	General Electric Company, Research and Development Center, Box 8, Schenectady, NY 12345
1	ATTN: Dr. R. J. Charles
1	Dr. C. D. Greskovich
1	Dr. S. Prochazka
	General Motors Corporation, AC Spark Plug Division, Flint, MI 48556
1	ATTN: Dr. M. Berg
	Georgia Institute of Technology, EES, Atlanta, GA 30332
1	ATTN: Mr. J. D. Walton
	GTE Laboratories, Waltham Research Center, 40 Sylvan Road, Waltham, MA 02154
1	ATTN: Dr. C. Quackenbush
1	Dr. W. H. Rhodes
	IIT Research Institute, 10 West 35th Street, Chicago, IL 60616
1	ATTN: Mr. S. Bortz, Director, Ceramics Research
1	Dr. D. Larsen
	Institut fur Werkstoff-Forschung, DFVLR, 505 Porz-Wahn, Linder Hohe, Germany
1	ATTN: Dr. W. Bunk
	Institut fur Werkstoff-Forschung, DFVLR, 5000 Koln 90(Porz), Linder Hohe, Germany
1	ATTN: Dr. Ing Jurgen Heinrich

No. of Copies	To
	International Harvester, Solar Division, 2200 Pacific Highway, P.O. Box 80966, San Diego, CA 92138
1	ATTN: Dr. A. Metcalfe
1	Ms. M. E. Gulden
	Jet Propulsion Laboratory, C.I.T., 4800 Oak Grove Drive, Pasadena, CA 91103
1	ATTN: Dr. Richard Smoak
	Kawecki Berylco Industries, Inc., P.O. Box 1462, Reading, PA 19603
1	ATTN: Mr. R. J. Longenecker
1	Mr. Edward Kraft, Product Development Manager, Industrial Sales Division, Kyocera International, Inc., 8611 Balboa Avenue, San Diego, CA 92123
	Martin Marietta Laboratories, 1450 South Rolling Road, Baltimore, MD 21227
1	ATTN: Dr. J. Venables
	Massachusetts Institute of Technology, Department of Metallurgy and Materials Science, Cambridge, MA 02139
1	ATTN: Prof. R. L. Coble
1	Prof. H. K. Bowen
1	Prof. W. D. Kingery
1	Prof. R. Cannon
	Materials Research Laboratories, P.O. Box 50, Ascot Vale, VIC 3032, Australia
1	ATTN: Dr. C. W. Weaver
	Midwest Research Institute, 425 Volker Boulevard, Kansas City, MO 64110
1	ATTN: Mr. Gordon W. Gross, Head, Physics Station
1	Dr. Howard Mizuhara, GTE-Wesgo, 477 Harbor Boulevard, Belmont, CA 94002
	Norton Company, Worcester, MA 01606
1	ATTN: Dr. N. Ault
1	Dr. M. L. Torti
	Pennsylvania State University, Materials Research Laboratory, Materials Science Department, University Park, PA 16802
1	ATTN: Prof. R. Roy
1	Prof. R. E. Newnham
1	Prof. R. E. Tressler
1	Prof. R. Bradt
1	Prof. V. S. Stubican
	Pratt and Whitney Aircraft, P.O. Box 2691, West Palm Beach, FL 33402
1	ATTN: Mr. Mel Mendelson
	PSC, Box 1044, APO San Francisco 96328
1	ATTN: MAJ A. Anthony Borges
	RIAS, Division of the Martin Company, Baltimore, MD 21203
1	ATTN: Dr. A. R. C. Westwood
	Rockwell International Science Center, 1049 Camino Dos Rios, Thousand Oaks, CA 91360
1	ATTN: Dr. F. Lange
	Royal Aircraft Establishment, Materials Department, R 178 Building, Farnborough, Hants, England
1	ATTN: Dr. N. Corney
	Shane Associates, Inc., 7821 Carrleigh Parkway, Springfield, VA 22152
1	ATTN: Dr. Robert S. Shane, Consultant

No. of Copies	To
	Silag Inc., P.O. Drawer H, Old Buncombe at Poplar Greer, SC 29651
1	ATTN: Dr. Bryant C. Bechtold
	Solar Turbine International, 2200 Pacific Coast Highway, San Diego, CA 92138
1	ATTN: Mr. Andrew Russel, Mail Zone R-1
	Stanford Research International, 333 Ravenswood Avenue, Menlo Park, CA 94025
1	ATTN: Dr. P. Jorgensen
1	Dr. D. Rowcliffe
	State University of New York at Stony Brook, Department of Materials Science, Long Island, NY 11790
1	ATTN: Prof. Franklin F. Y. Wang
	TRW Defense and Space Systems Group, Redondo Beach, CA 90278
1	ATTN: Francis E. Fendell
	United Technologies Research Center, East Hartford, CT 06108
1	ATTN: Dr. J. Brennan
1	Dr. F. Galasso
	University of California, Lawrence Livermore Laboratory, P. O. Box 808, Livermore, CA 94550
1	ATTN: Mr. R. Landingham
1	Dr. C. F. Cline
	University of Florida, Department of Materials Science and Engineering, Gainesville, FL 32601
1	ATTN: Dr. L. Hench
	University of Massachusetts, Department of Mechanical Engineering, Amherst, MA 01003
1	ATTN: Prof. K. Jakus
1	Prof. J. Ritter
	University of Newcastle Upon Tyne, Department of Metallurgy and Engineering Materials, Newcastle Upon Tyne, NEI 7 RU, England
1	ATTN: Prof. K. H. Jack
	University of Washington, Ceramic Engineering Division, FB-10, Seattle, WA 98195
1	ATTN: Prof. James I. Mueller
	Virginia Polytechnic Institute, Department of Materials Engineering, Blacksburg, VA 24061
1	Prof. D. P. H. Hasselman
	Westinghouse Electric Corporation, Research Laboratories, Pittsburgh, PA 15235
1	ATTN: Dr. R. J. Bratton
1	Dr. B. Rossing
1	Mr. Joseph T. Bailey, 3M Company, Technical Ceramic Products Division, 3M Center, Building 207-1W, St. Paul, MN 55101
1	Dr. Jacob Stiglich, Dart Industries/San Fernando Laboratories, 10258 Norris Avenue, Pacoima, CA 91331
1	Dr. J. Petrovic - CMR-5, Mail Stop 730, Los Alamos Scientific Laboratories, Los Alamos, NM 87545
1	Mr. R. J. Zentner, EAI Corporation, 198 Thomas Johnson Drive, Suite 16, Frederick, MD 21701
	Director, Army Materials and Mechanics Research Center, Watertown, MA 02172
2	ATTN: DRXMR-PL
2	Authors

Army Materials and Mechanics Research Center,
Watertown, Massachusetts 02172
FRACTURE ANALYSIS OF REACTION-BONDED
SILICON NITRIDE TURBINE SHROUDS -
Donald R. Messier, Liselotte J. Schioler,
George D. Quinn, and James C. Napier

Technical Report AMMRC TR 82-43, June 1982, 38 pp -
illus-tables, D/A Project 1L763702 DG1105
AMCMS Code 623702.G1100

AD__________

UNCLASSIFIED
UNLIMITED DISTRIBUTION

Key Words

Silicon nitride
Ceramics
Gas turbine engine

Reaction-bonded silicon nitride turbine shrouds were examined after engine rig testing to determine failure mechanisms and evaluate material quality. Bend test specimens machined from the shrouds were approximately equal in strength to specimens cut from flat billets of virgin material. While most component and bend specimen fractures initiated at surfaces, internal origins were observed in some cases. Fracture mechanics analysis of the bend test data yielded a value of K_{Ic} = 1.79 $MN/m^{3/2}$ in agreement with literature data. Fracture mirror measurements indicated that shrouds failed at stresses approximately three times less than bend specimens. Probable causes for this were gross machining defects, size effects, and possible residual stresses.

Army Materials and Mechanics Research Center,
Watertown, Massachusetts 02172
FRACTURE ANALYSIS OF REACTION-BONDED
SILICON NITRIDE TURBINE SHROUDS -
Donald R. Messier, Liselotte J. Schioler,
George D. Quinn, and James C. Napier

Technical Report AMMRC TR 82-43, June 1982, 38 pp -
illus-tables, D/A Project 1L763702 DG1105
AMCMS Code 623702.G1100

AD__________

UNCLASSIFIED
UNLIMITED DISTRIBUTION

Key Words

Silicon nitride
Ceramics
Gas turbine engine

Reaction-bonded silicon nitride turbine shrouds were examined after engine rig testing to determine failure mechanisms and evaluate material quality. Bend test specimens machined from the shrouds were approximately equal in strength to specimens cut from flat billets of virgin material. While most component and bend specimen fractures initiated at surfaces, internal origins were observed in some cases. Fracture mechanics analysis of the bend test data yielded a value of K_{Ic} = 1.79 $MN/m^{3/2}$ in agreement with literature data. Fracture mirror measurements indicated that shrouds failed at stresses approximately three times less than bend specimens. Probable causes for this were gross machining defects, size effects, and possible residual stresses.

Army Materials and Mechanics Research Center,
Watertown, Massachusetts 02172
FRACTURE ANALYSIS OF REACTION-BONDED
SILICON NITRIDE TURBINE SHROUDS -
Donald R. Messier, Liselotte J. Schioler,
George D. Quinn, and James C. Napier

Technical Report AMMRC TR 82-43, June 1982, 38 pp -
illus-tables, D/A Project 1L763702 DG1105
AMCMS Code 623702.G1100

AD__________

UNCLASSIFIED
UNLIMITED DISTRIBUTION

Key Words

Silicon nitride
Ceramics
Gas turbine engine

Reaction-bonded silicon nitride turbine shrouds were examined after engine rig testing to determine failure mechanisms and evaluate material quality. Bend test specimens machined from the shrouds were approximately equal in strength to specimens cut from flat billets of virgin material. While most component and bend specimen fractures initiated at surfaces, internal origins were observed in some cases. Fracture mechanics analysis of the bend test data yielded a value of K_{Ic} = 1.79 $MN/m^{3/2}$ in agreement with literature data. Fracture mirror measurements indicated that shrouds failed at stresses approximately three times less than bend specimens. Probable causes for this were gross machining defects, size effects, and possible residual stresses.

Army Materials and Mechanics Research Center,
Watertown, Massachusetts 02172
FRACTURE ANALYSIS OF REACTION-BONDED
SILICON NITRIDE TURBINE SHROUDS -
Donald R. Messier, Liselotte J. Schioler,
George D. Quinn, and James C. Napier

Technical Report AMMRC TR 82-43, June 1982, 38 pp -
illus-tables, D/A Project 1L763702 DG1105
AMCMS Code 623702.G1100

AD__________

UNCLASSIFIED
UNLIMITED DISTRIBUTION

Key Words

Silicon nitride
Ceramics
Gas turbine engine

Reaction-bonded silicon nitride turbine shrouds were examined after engine rig testing to determine failure mechanisms and evaluate material quality. Bend test specimens machined from the shrouds were approximately equal in strength to specimens cut from flat billets of virgin material. While most component and bend specimen fractures initiated at surfaces, internal origins were observed in some cases. Fracture mechanics analysis of the bend test data yielded a value of K_{Ic} = 1.79 $MN/m^{3/2}$ in agreement with literature data. Fracture mirror measurements indicated that shrouds failed at stresses approximately three times less than bend specimens. Probable causes for this were gross machining defects, size effects, and possible residual stresses.

Army Materials and Mechanics Research Center,
Watertown, Massachusetts 02172
FRACTURE ANALYSIS OF REACTION-BONDED
SILICON NITRIDE TURBINE SHROUDS -
Donald R. Messier, Liselotte J. Schioler,
George D. Quinn, and James C. Napier

Technical Report AMMRC TR 82-43, June 1982, 38 pp -
illus-tables, D/A Project 1L763702 DG1105
AMCMS Code 623702.G1100

AD________________

UNCLASSIFIED
UNLIMITED DISTRIBUTION

Key Words

Silicon nitride
Ceramics
Gas turbine engine

Reaction-bonded silicon nitride turbine shrouds were examined after engine rig testing to determine failure mechanisms and evaluate material quality. Bend test specimens machined from the shrouds were approximately equal in strength to specimens cut from flat billets of virgin material. While most component and bend specimen fractures initiated at surfaces, internal origins were observed in some cases. Fracture mechanics analysis of the bend test data yielded a value of K_{Ic} = 1.79 $MN/m^{3/2}$ in agreement with literature data. Fracture mirror measurements indicated that shrouds failed at stresses approximately three times less than bend specimens. Probable causes for this were gross machining defects, size effects, and possible residual stresses.

Army Materials and Mechanics Research Center,
Watertown, Massachusetts 02172
FRACTURE ANALYSIS OF REACTION-BONDED
SILICON NITRIDE TURBINE SHROUDS -
Donald R. Messier, Liselotte J. Schioler,
George D. Quinn, and James C. Napier

Technical Report AMMRC TR 82-43, June 1982, 38 pp -
illus-tables, D/A Project 1L763702 DG1105
AMCMS Code 623702.G1100

AD________________

UNCLASSIFIED
UNLIMITED DISTRIBUTION

Key Words

Silicon nitride
Ceramics
Gas turbine engine

Reaction-bonded silicon nitride turbine shrouds were examined after engine rig testing to determine failure mechanisms and evaluate material quality. Bend test specimens machined from the shrouds were approximately equal in strength to specimens cut from flat billets of virgin material. While most component and bend specimen fractures initiated at surfaces, internal origins were observed in some cases. Fracture mechanics analysis of the bend test data yielded a value of K_{Ic} = 1.79 $MN/m^{3/2}$ in agreement with literature data. Fracture mirror measurements indicated that shrouds failed at stresses approximately three times less than bend specimens. Probable causes for this were gross machining defects, size effects, and possible residual stresses.

Army Materials and Mechanics Research Center,
Watertown, Massachusetts 02172
FRACTURE ANALYSIS OF REACTION-BONDED
SILICON NITRIDE TURBINE SHROUDS -
Donald R. Messier, Liselotte J. Schioler,
George D. Quinn, and James C. Napier

Technical Report AMMRC TR 82-43, June 1982, 38 pp -
illus-tables, D/A Project 1L763702 DG1105
AMCMS Code 623702.G1100

AD________________

UNCLASSIFIED
UNLIMITED DISTRIBUTION

Key Words

Silicon nitride
Ceramics
Gas turbine engine

Reaction-bonded silicon nitride turbine shrouds were examined after engine rig testing to determine failure mechanisms and evaluate material quality. Bend test specimens machined from the shrouds were approximately equal in strength to specimens cut from flat billets of virgin material. While most component and bend specimen fractures initiated at surfaces, internal origins were observed in some cases. Fracture mechanics analysis of the bend test data yielded a value of K_{Ic} = 1.79 $MN/m^{3/2}$ in agreement with literature data. Fracture mirror measurements indicated that shrouds failed at stresses approximately three times less than bend specimens. Probable causes for this were gross machining defects, size effects, and possible residual stresses.

Army Materials and Mechanics Research Center,
Watertown, Massachusetts 02172
FRACTURE ANALYSIS OF REACTION-BONDED
SILICON NITRIDE TURBINE SHROUDS -
Donald R. Messier, Liselotte J. Schioler,
George D. Quinn, and James C. Napier

Technical Report AMMRC TR 82-43, June 1982, 38 pp -
illus-tables, D/A Project 1L763702 DG1105
AMCMS Code 623702.G1100

AD________________

UNCLASSIFIED
UNLIMITED DISTRIBUTION

Key Words

Silicon nitride
Ceramics
Gas turbine engine

Reaction-bonded silicon nitride turbine shrouds were examined after engine rig testing to determine failure mechanisms and evaluate material quality. Bend test specimens machined from the shrouds were approximately equal in strength to specimens cut from flat billets of virgin material. While most component and bend specimen fractures initiated at surfaces, internal origins were observed in some cases. Fracture mechanics analysis of the bend test data yielded a value of K_{Ic} = 1.79 $MN/m^{3/2}$ in agreement with literature data. Fracture mirror measurements indicated that shrouds failed at stresses approximately three times less than bend specimens. Probable causes for this were gross machining defects, size effects, and possible residual stresses.

END

FILMED